Journal of Pharmaceutical Analysis 15 (2025) 101132

Contents lists available at ScienceDirect

Journal of Pharmaceutical Analysis

journal homepage: www.elsevier.com/locate/jpa

Original article

Discovery of E0199: A novel compound targeting both peripheral Na_V and K_V7 channels to alleviate neuropathic pain

Boxuan Zhang [a], Xiaoxing Shi [b], Xingang Liu [a], Yan Liu [c], Xuedong Li [a], Qi Wang [d], Dongyang Huang [b], Weidong Zhao [b], Junru Cui [e], Yawen Cao [b], Xu Chai [b], Jiahao Wang [b], Yang Zhang [a, ***], Xiangyu Wang [f, g, **], Qingzhong Jia [a, *]

[a] Department of Pharmaceutical Chemistry, College of Pharmacy, Hebei Medical University, Shijiazhuang, 050017, China
[b] Department of Pharmacology, College of Basic Medical, Hebei Medical University, Shijiazhuang, 050017, China
[c] Department of Pharmaceutical Experimental Teaching Center, College of Pharmacy, Hebei Medical University, Shijiazhuang, 050017, China
[d] Shijiazhuang Xianyu Digital Biotechnology Co., Ltd., College of Software, Hebei Normal University, Shijiazhuang, 050024, China
[e] The Center for New Drug Safety Evaluation and Research, Hebei Medical University, Shijiazhuang, 050017, China
[f] Hebei Medical University Postdoctoral Mobile Station of Basic Medical, Hebei Medical University, Shijiazhuang, 050017, China
[g] Departments of Clinic Pharmacy, College of Pharmacy, Hebei Medical University, Shijiazhuang, 050017, China

ARTICLE INFO

Article history:
Received 2 May 2024
Received in revised form
7 October 2024
Accepted 22 October 2024
Available online 25 October 2024

Keywords:
Neuropathic pain
Na_V channel
K_V7 channel
Dorsal root ganglia

ABSTRACT

This research study focuses on addressing the limitations of current neuropathic pain (NP) treatments by developing a novel dual-target modulator, E0199, targeting both $Na_V1.7$, $Na_V1.8$, and $Na_V1.9$ and K_V7 channels, a crucial regulator in controlling NP symptoms. The objective of the study was to synthesize a compound capable of modulating these channels to alleviate NP. Through an experimental design involving both *in vitro* and *in vivo* methods, E0199 was tested for its efficacy on ion channels and its therapeutic potential in a chronic constriction injury (CCI) mouse model. The results demonstrated that E0199 significantly inhibited $Na_V1.7$, $Na_V1.8$, and $Na_V1.9$ channels with a particularly low half maximal inhibitory concentration (IC_{50}) for $Na_V1.9$ by promoting sodium channel inactivation, and also effectively increased $K_V7.2/7.3$, $K_V7.2$, and $K_V7.5$ channels, excluding $K_V7.1$ by promoting potassium channel activation. This dual action significantly reduced the excitability of dorsal root ganglion neurons and alleviated pain hypersensitivity in mice at low doses, indicating a potent analgesic effect without affecting heart and skeletal muscle ion channels critically. The safety of E0199 was supported by neurobehavioral evaluations. Conclusively, E0199 represents a ground-breaking approach in NP treatment, showcasing the potential of dual-target small-molecule compounds in providing a more effective and safe therapeutic option for NP. This study introduces a promising direction for the future development of NP therapeutics.

1. Introduction

Neuropathic pain (NP) is a common condition caused by lesions or diseases of the somatosensory nervous system [1]. Clinical examples of NP include trigeminal neuralgia, postherpetic neuralgia, and central post-stroke pain [2–4]. The pathogenesis of NP is complex and can stem from various mechanisms, such as anatomical changes and functional impairment. Peripheral and central sensitisation, malfunctioning descending inhibitory systems, activation of spinal glial cells, and changes in ion channels are the common mechanisms [5]. Analgesics such as tricyclic antidepressant (TCA) nortriptyline, 5-hydroxytryptamine norepinephrine reuptake inhibitor duloxetine, calcium channel 2-ligand gabapentin, sodium channel blocker lidocaine, and opioid agonist morphine-controlled release tablets are commonly used for the treatment of NP in clinical trials [2]. These medications have a limited therapeutic effect, and prolonged use can lead to adverse effects such as immunological disorders and physical dependence [1,2]. Therefore, the development of novel

Peer review under responsibility of Xi'an Jiaotong University.
* Corresponding author.
** Corresponding author. Hebei Medical University Postdoctoral Mobile Station of Basic Medical, Hebei Medical University, Shijiazhuang, 050017, China.
*** Corresponding author.
E-mail addresses: zhangyang@hebmu.edu.cn (Y. Zhang), 19301689@hebmu.edu.cn (X. Wang), 17200912@hebmu.edu.cn (Q. Jia).

https://doi.org/10.1016/j.jpha.2024.101132

and potent medications for the treatment of NP is urgently required.

Sodium channels are important targets for the development of analgesic medications as they are essential for the release of action potential (AP) [6]. $Na_V1.7$ channels regulate the AP threshold and contribute significantly to its upstroke [7]. In addition, $Na_V1.8$ contributes to most of the sodium current during the depolarisation phase of the AP in neurons [8]. Moreover, $Na_V1.9$ affects the depolarisation process of the resting membrane potential (RMP) and the number of spontaneous and evoked discharges [9]. There are nine subtypes of voltage-gated sodium channels, including $Na_V1.4$ mainly distributed in the skeletal muscles, $Na_V1.5$ in the heart [1], and $Na_V1.7$, $Na_V1.8$, and $Na_V1.9$ in the peripheral nervous system [6,7,10]. Sodium voltage-gated channel alpha subunit 9 (SCN9A), coding $Na_V1.7$ channel, inactivation mutations cause congenital pain insensitivity, whereas SCN9A gain-of function mutations cause various pain syndromes, such as inherited erythromelalgia, paroxysmal extreme pain disorder, and small-fibre neuropathy [11]. Mutations in the SCN10A, coding $Na_V1.8$ channel, gene can cause small-fibre neuropathy, and mutations in SCN11A, coding $Na_V1.9$ channel, can cause congenital pain insensitivity [9,11–14]. Therefore, the development of analgesics targeting channels such as $Na_V1.7$, $Na_V1.8$, and $Na_V1.9$ is a top priority.

Currently, small-molecule blockers targeting $Na_V1.7$, such as PF-05089771, have undergone clinical studies; however, their analgesic effects are unsatisfactory [15]. Besides, lacosamide, developed by Union Chimique Belge Pharm (UCB), has been approved as an adjunctive therapy for treating partial-onset seizures in several countries worldwide. Nonetheless, reports are indicating less effective pain treatment outcomes [16–18]. Small molecule inhibitors of $Na_V1.7$, such as CNV1014802, have demonstrated effectiveness in treating NP in rodent models [19,20]. $Na_V1.8$ blockers, such as PF-01247324, are highly effective in treating inflammatory pain and spinal nerve ligation pain in rodent models [20]. In addition to small molecules such as A-887826, which exhibits analgesic activity in rodent models, there is VX-150, which has progressed to the clinical trial stage [21,22]. The $Na_V1.9$ blocker ANP-230 alleviates pain hypersensitivity in mice with $Na_V1.9^{R222S}$ mutations associated with familial episodic pain syndrome [23]. Several research groups worldwide are actively engaged in the development of inhibitors targeting $Na_V1.7$, $Na_V1.8$, and $Na_V1.9$, making these highly promising targets in the current landscape of small-molecule drug development.

The K_V7 channels play a crucial role in pain regulation by influencing the RMP, thereby affecting neuronal excitability [6,24–28]. This channel has recently emerged as a key target for the development of novel analgesics. The K_V7 channels are classified into five subtypes, with $K_V7.1$ primarily found in the heart, $K_V7.4$ in the inner ear, and $K_V7.2$, $K_V7.3$, and $K_V7.5$ commonly co-expressed in the nervous system [24,25]. Reportedly, animals with the $K_V7.2$ channel knocked out in the dorsal root ganglia (DRG) produce hyperalgesia, and the $K_V7.2$ functional gain mutation can alleviate the pain of "burning man syndrome" [20,29]. While novel K_V7 agonists, such as retigabine, exhibit broad effectiveness, they also pose significant risks when used to treat postherpetic neuralgia. Concerns related to hepatotoxicity have prompted the withdrawal of flupirtine from the market, and SCR2682 cells are not currently used in clinical studies. The effectiveness of the mallotoxin isovaleric acid (E)-2-dodecenal in pain models is yet to be verified [30]. Previously, our research group developed the small molecule QO-58, which alleviates NP by increasing the threshold for chronic constriction injury (CCI) [31].

The development of drugs for multiple targets is feasible because most NP pathways are complex and targeting a single way only can provide limited pain relief. Currently, there is no medication available that specifically blocks Na_V channels. We focused on co-regulating the Na_V channels and K_V7 channels and designated E0199 as a dual-action compound with the ability to activate the K_V7 channel while simultaneously blocking the $Na_V1.7$, $Na_V1.8$, and $Na_V1.9$ channels. In addition, we confirmed its biological activity in animals and cellular models.

2. Materials and methods

2.1. DNA constructs

Plasmids encoding human $K_V7.5$ and $Na_V1.1$ (NM_001160132.2 and NM_001165963.4) were kindly provided by Hebei Medical University (Shijiazhuang, China). $Na_V1.6$ (NM_014191.4) were kindly provided by Chinese Academy of Sciences (Shanghai, China).

2.2. Cells and transfection

Stable CHO cells expressing $K_V7.1$, $K_V7.2$, $K_V7.4$, and $K_V7.2/7.3$, and stable HEK cells expressing $Na_V1.5$ and $Na_V1.7$ channels were kindly provided by Hebei Medical University. Stable HEK cells expressing $Na_V1.4$ channels were kindly provided by Qingdao University (Qingdao, China).

For transfection of cells, a mixture of 500 ng of plasmid, 300 ng of green fluorescent protein (GFP), and 1.5 μL of FuGENE® HD Transfection Reagent (Promega (Beijing) Biotech Co., Ltd., Beijing, China) was prepared in 520 μL of DMEM-F12 (Gibco Life Technologies, Grand Island, NY, USA). The mixture was then applied to the cell culture wells and incubated for 24–48 h. Recordings were made after successful transfection.

For DRG neurons, this method has been previously described in detail [32]. $Na_V1.8$ and $Na_V1.9$ currents as well as APs in control were recorded in medium- and small-diameter DRG neurons of untreated rats. AP in model was recorded in medium- and small-diameter DRG neurons of CCI rats.

2.3. Whole-cell patch clamp recordings

Whole-cell clamp recordings were performed at room temperature (25 °C) to measure transient sodium current and APs using the amplifier (EPC 10) and PatchMaster. The patch pipettes were pulled from borosilicate capillaries (2–4 MΩ, with solution). Pipette capacitance compensation and whole-cell membrane capacitance of mediated current need to be compensated optimally. The series resistance was compensated by 70%–80%. The signal low-pass filtering frequency was set at 5 kHz and the acquisition rate at 20 kHz. The cells in the recording chamber (300 μL) was at a rate of 3–4 mL/min. All drugs were administered by perfusion system. The solution exchange time was 1–2 s. Data were sampled 2–3 min after achieving whole-cell configuration. Membrane currents or APs were measured 3 min before drug administration.

2.3.1. APs recording

The pipette solution contained the following components: 140 mM KCl, 1 mM $CaCl_2$, 2 mM $MgCl_2$, 10 mM *N*-2-hydroxyethylpiperazine-*N*-ethane-sulphonicacid (HEPES), and 11 mM ethyleneglycol-bis(2-aminoethylether)-*N*,*N*,*N*′,*N*′-tetra-acetic acid (EGTA), with pH adjusted to 7.4 using KOH. The external solution contained the following components: 150 mM NaCl, 5 mM KCl, 2.5 mM $CaCl_2$, 1 mM $MgCl_2$, 10 mM glucose, and 10 mM HEPES, with pH adjusted to 7.4 using NaOH. All chemicals are purchased from Sigma-Aldrich Corporation (Shanghai, China). The effects of treatment with carbamazepine (CBZ, 30 μM), retigabine (RTG, 10 μM), RTG (5 μM) + CBZ (15 μM), and E0199 (1, 3, and 10 μM) were recorded. CBZ was purchased by MedChemExpress LLC (Herndon, VA, USA). RTG was purchased by Shanghai Titan

Technology Co., Ltd. (Shanghai, China). DRG neurons were subjected to currents of different intensities (ranging from 0 to 600 pA, with a gradient of 100 pA).

2.3.2. $Na_V1.8$: sodium current recording

The composition of the pipette solution was as follows: 70 mM $CsCl_2$, 30 mM NaCl, 30 mM tetraethylammonium chloride (TEA-Cl), 10 mM EGTA, 1 mM $CaCl_2$, 2 mM $MgCl_2$, 10 mM HEPES, 5 mM D-glucose, 2 mM adenosine 5′-triphosphate disodium salt (Na_2ATP), and 0.05 mM guanosine triphosphate (GTP), with pH adjusted to 7.3 using CsOH. The composition of the external solution was as follows: 80 mM NaCl, 50 mM choline-Cl, 30 mM TEA-Cl, 2 mM $CaCl_2$, 0.2 mM $CdCl_2$, 10 mM HEPES, and 5 mM D-glucose. The pH of tetrodotoxin (TTX, 500 nM) was adjusted to 7.4 using NaOH. TTX was purchased from Taizhou Kangte Biological Engineeering Company (Taizhou, China). All chemicals were purchased from Sigma-Aldrich Corporation. A prepulse voltage of −44 mV (500 ms) was set, and subsequently the $Na_V1.8$ current was excited using a series of depolarisations in 50 ms steps (−80 to 0 mV in 5 mV increments) [33,34].

2.3.3. $Na_V1.9$: sodium current recording

The composition of the pipette solution contained was as follows: 100 mM CsCl, 8 mM NaCl, 30 mM CsF, 5 mM EGTA, 2.4 mM $CaCl_2$, 1 mM $MgCl_2$, 10 mM HEPES, 4 mM Na_2ATP, and 0.4 mM GTP. The pH was adjusted to 7.3 using CsOH. The external solution was comprised of: 40 mM NaCl, 100 mM choline-Cl, 3 mM KCl, 2.5 mM $CaCl_2$, 1 mM $MgCl_2$, 10 mM HEPES, 10 mM glucose, 0.05 mM $LaCl_3$, and 100 nM TTX. All chemicals are purchased from Sigma-Aldrich Corporation. The pre-set voltage of −100 mV, 50 ms was used to apply a series of 50 ms steps of depolarisation excitations (ranging from −100 to −35 in 5 mV increments) to eliminate the $Na_V1.8$ current.

2.3.4. $Na_V1.7$, $Na_V1.4$, and $Na_V1.5$ sodium current recording

The pipette solution contained the following components: 145 mM CsF, 5.6 mM NaF, and 5 mM HEPES, with a pH adjusted to 7.3 using CsOH. The external solution was composed of components: 140 mM NaCl, 5.4 mM KCl, 1.8 mM $CaCl_2$, 0.5 mM $MgCl_2$, 5 mM HEPES, 5.5 mM D-glucose, and 0.4 mM NaH_2PO_4, with pH adjusted to 7.4 using NaOH. All chemicals are purchased from Sigma-Aldrich Corporation. The protocol was set to incrementally increase from −80 to 20 mV in increments of 10 mV steps to activate the $Na_V1.7$ current, with each stimulus lasting for 50 ms.

2.3.5. $K_V7.2$, $K_V7.1$, $K_V7.2/7.3$, $K_V7.4$, and $K_V7.5$ channels current recording

The pipette and external solutions were the same as those for the DRG AP. The protocol was set to increase from −120 to 40 mV (increase of 10 mV each time) to evoke the series of K_V7 currents, and each time stimulation lasts for 2000 ms.

2.4. Animals

Sprague Dawley (SD) rats were used for the electrophysiological studies of DRG neurons, and the test of concentration in tissues. Male C57 (8−10 weeks old; Beijing Vital River Laboratory Animal Technology Co., Ltd., Beijing, China) mice for all of the pain behavior and other neurobehavior tests and pharmacological studies. Animals were group housed in a 12 h light/dark cycle at 22 ± 1 °C with free access to food and water. All animal experiments had comply with the Animal Research: Reporting of *In Vivo* Experiments (ARRIVE) guidelines and been carried out in accordance with the U.K. Animals Act, 1986 and associated guidelines, EU Directive 2010/63/EU for animal experiments, and the National Research Council's Guide for the Care and Use of Laboratory Animals [35−38]. The Animal Ethics Committee of Hebei Medical University approved all animal experiments (Approval No.: IACUC-Hebyd AP2023033).

2.5. Animal models of pain and drug administration

We used isoflurane anaesthesia to induce CCI in male C57 mice to create the NP model. Following CCI surgery, cotton mats and food were provided to comfort the animals, and NP behaviours were evaluated every three days. NP following CCI was treated with intraperitoneal (i.p.) injections of CBZ (20 mg/kg), RTG (10 mg/kg), RTG (5 mg/kg) + CBZ (10 mg/kg), or E0199 (1, 5, and 20 mg/kg) at 9 a.m. every day (between 11 and 30 days).

2.6. Behavioural testing

2.6.1. Pain threshold test

The animals were acclimatised to their surroundings for at least two days. Every behaviour underwent blind testing. Sensitivity to mechanical stimulation was measured using von Frey hairs (0.02−2.56 g, Stoelting, Chicago, IL, USA). A Hargreaves radiant heat device (IITC Life Science Inc., Los Angeles, CA, USA) was used to measure thermal sensitivity. The basal paw withdrawal latency for the radiant heat test was set at a 30 s cut-off to avoid tissue damage. The cold sensitivity was measured using a cold plate at 4 °C. The basal paw withdrawal latency was set at a 60 s cut-off to prevent tissue damage.

2.6.2. Open-field experiment and high-plus maze

In open-field experiment, the mouse was positioned with its head facing outward in a stationary corner and then introduced to the box aperture. The test lasted for 5 min. The camera and Smart 3.0 software (Mobile Datum, Shanghai, China) captured the entry of mice into the central area. All measurements, including distance, arrival time, and duration of stay in the central region, were recorded. In high-plus maze, the test mouse was placed with its head facing the dark arm at the junction of the open and dark arms of the high-plus maze. The test lasted for 10 min. Smart 3.0 (Mobile Datum) was used to record the time and number of entries into open or dark arms [39].

2.7. Dual-target drug screening based on $K_V7.2$ and $Na_V1.7$ channel proteins: system preparation and virtual screening

2.7.1. System preparation

According to the commercial suppliers and in-house molecular library, we have integrated a total of approximately 35,000 small molecules to be screened. Afterwards, the molecular dataset underwent conformational and energy optimization, involving the creation of ionisation states, tautomerization, and energy minimization. Then, the crystal structures of $K_V7.2$ (Protein Data Bank (PDB) ID: 7CR2, resolution: 3.20 Å) and $Na_V1.7$ (PDB ID: 5EK0; resolution: 3.53 Å) were fetched from the PDB, which were further processed by “Prepare protein” tool under the “Macromolecules” module, including removing water molecules, deleting heteroatoms, hydrogenating, building loop regions, and protonating the protein structures, and so on.

2.7.2. Virtual screening

The virtual screening scheme mainly consisted of the following steps: rapid screening via deep learning algorithms, re-evaluation based on molecular docking, scaffold analysis, binding free energy evaluation using molecular dynamics simulation, and biological activity assessment. First, the ligand-target binding affinity of the constructed molecular library was evaluated based on the simple-structured graph neural network (SS-GNN) [40] deep learning

model previously reported by our group, and a total of 210 molecules were retained based on conformational evaluation and scoring. The top 210 molecules were further comprehensively assessed by molecular docking through LibDock and CDOCKER modules, and molecules with consistent docking scores were used for subsequent skeleton cluster analysis and molecular dynamic simulation. Furthermore, the SA_score plug-in RDKit was applied to evaluate molecular complexity to further judge the difficulty of chemical synthesis.

2.8. Determination of drug concentration in tissue

In untreated rats, blank blood need to be collected, and brain, DRG, liver and kidney were collected after decapitation. Rats in the administration group were given caudal intravenous administration (1 mg/kg). At 5 min, 15 min, 0.5 h, 1 h, and 2 h, we used isoflurane anaesthesia and took blood from the abdominal aorta, then we severed the head, and took the brain, liver and kidney, with the ice box used to transfer the tissue to the −80 °C refrigerator. We made the pretreatment of tissue, and then we prepared the sample solution for liquid chromatograph-mass spectrometry (LC-MS) analysis.

2.9. Statistical analyses

We state that all of the statistical analysis that the MS conforms to the guidance described in Curtis et al. [41], and we had considered in blinding and randomness, as well as power analysis, with statistical analysis being conducted on sample numbers of a minimum of 5. All data are expressed as mean ± standard error of the mean (SEM), as indicated in the figure legends. Statistical analyses were performed using Prism GraphPad. Biochemical and behavioural data were analyzed using a two-tailed Student's *t*-test (two groups) or two-way analysis of variance (ANOVA), followed by a post-hoc Bonferroni test. Electrophysiological data were tested processed one-way ANOVA (for multiple comparisons) or two-way ANOVA.

3. Results

3.1. Screening of active small molecular compounds targeting both $Na_V1.7$ and $K_V7.2$ channels

We used the SS-GNN algorithm to perform virtual screening on a library of approximately 35,000 small molecular compounds based on the crystal structures of $K_V7.2$ and $Na_V1.7$. The screening process identified 210 small-molecule compounds with high scores in both the $K_V7.2$ and $Na_V1.7$ systems, as detailed in (Supplementary data, Fig. S1, and Table S1). The LibDock and CDOCKER modules in Discover Studio 2020 were used to score these compounds. Subsequently, cluster analysis was performed, and three types of molecular skeletons with research value were mainly identified: pyrazolo [1,5-*a*]pyrimidin-7(4*H*)-one, *N*-(1,2,4-thiadiazol-5-yl) benzenesulfonamide, and 3-(piperazin-1-ylmethyl)-1,2,4-oxadiazole (Fig. 1 and Table 1) (retain the first letter and the last four digits). The top 20 compounds with high composite scores were synthesized and individually tested for activity using electrophysiological patch clamp assays at 20 μmol/L and the results of the electrophysiological activity validation are presented in Table 1. The top 5 compounds inhibiting $Na_V1.7$ channel activity were E0199 > QO-72 > QO-58 > QO-26 > JZJ003. At equivalent doses, the top 5 compounds for opening the $K_V7.2$ channel were E0199 > QO-72 > QO-58 > E0304 > QO-40 (Table 1). E0199 exhibited the highest potency and was selected for the total synthesis because of its strong effect on both the $Na_V1.7$ and $K_V7.2$ channels, and its subtype selectivity and pain-relieving mechanisms were further studied.

3.2. Preparation of compound E0199 in synthesis

Initially, *N*-benzylethanamine (**SM1**) was dissolved in dichloromethane (DCM) and then cooled to 0 °C. Triethylamine (TEA) and DCM solution of ethyl 4-chloro-4-oxobutanoate (**SM2**) were added to the above solution respectively. The reaction was allowed to

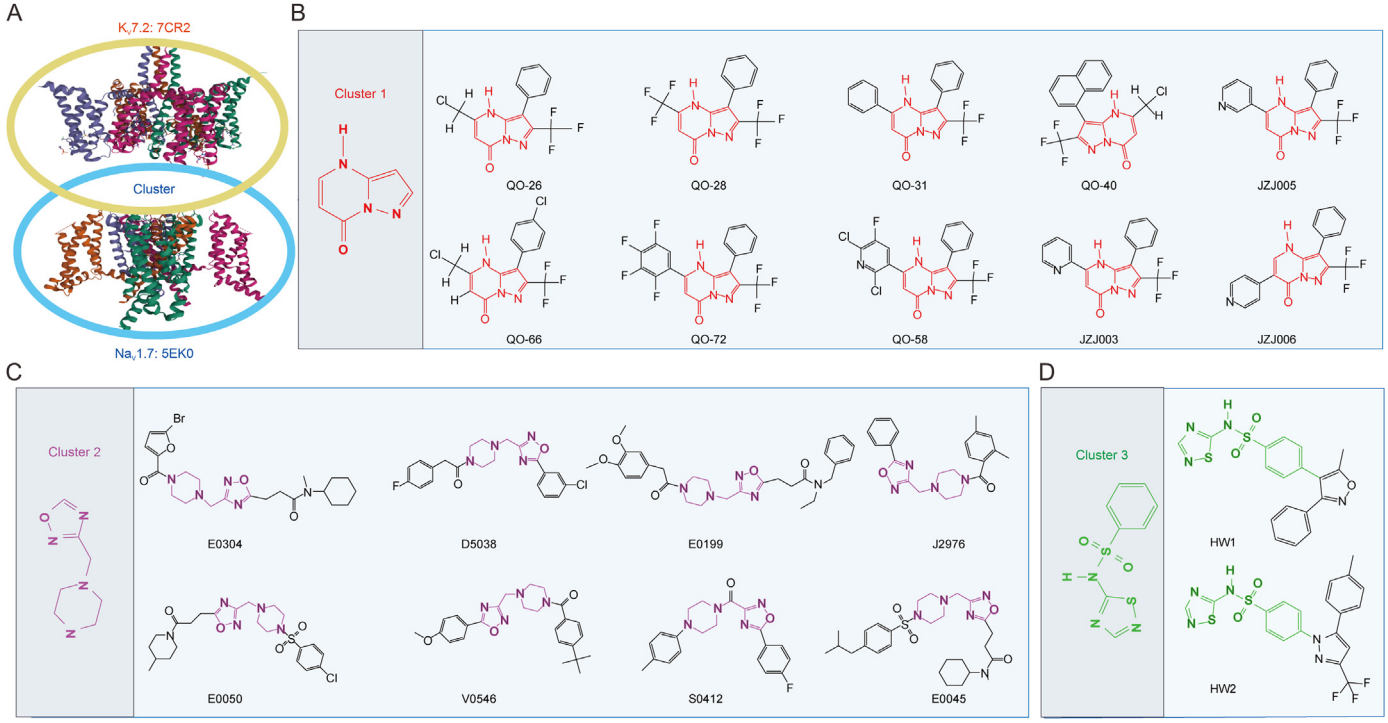

Fig. 1. Three series of small molecular compounds obtained by clustering the skeleton.

Table 1
Screening of active small molecular compounds targeting both $Na_V1.7$ and $K_V7.2$ channels ($n = 6$).

Name	Smiles	LibDockScore_5EK0	|CDOCKER_ENERGY|_5EK0	LibDockScore_7CR2	|CDOCKER_ENERGY|_7CR2	Inhibition of $Na_V1.7$ current (20 μM)	Increase of $K_V7.2$ current (20 μM)
E0050	O=S(N(CC1)CCN1CC2=NOC(CCC(N3CCC(C)CC3)=O)=N2) (C4=CC=C(Cl)C=C4)=O	166.798	46.4313	159.099	40.3233	0.24 ± 0.04	1.14 ± 0.12
E0199	COC1=C(OC)C=CC(CC(N2CCN(CC3=NOC(CCC(N(CC)CC4=CC=CC=C4)=O)=N3)CC2)=O)=C1	166.220	36.3446	159.685	30.7349	**0.52 ± 0.06**	**2.08 ± 0.10**
E0045	CC(C)CC1=CC=C(S(N2CCN(CC3=NOC(CCC(N(C)C4CCCCC4)=O)=N3)CC2) (=O)=O)C=C1	161.665	50.6015	159.878	33.9165	0.28 ± 0.05	1.08 ± 0.08
D5038	O=C(N1CCN(CC2=NOC(C3=CC=CC(Cl)=C3)=N2)CC1)CC4=CC=C(F)C=C4	149.643	30.8385	139.429	28.2026	0.01 ± 0.03	1.08 ± 0.06
E0304	O=C(N(C1CCCCC1)C)CCC2=NC(CN(CC3)CCN3C(C4=CC=C(Br)O4)=O)=NO2	147.654	35.7927	146.701	31.63	0.02 ± 0.02	1.22 ± 0.11
JZJ006	O=C1C(C2=CC=NC=C2)=CNC3=C(C4=CC=CC=C4)C(C(F) (F)F)=NN31	137.943	12.156	123.572	16.1007	0.26 ± 0.07	1.12 ± 0.07
HW2	O=S(C1=CC=C (N2C(C3=CC=C(C)C=C3)=CC(C(F) (F)F)=N2)C=C1) (N ([H])C4=NC=NS4)=O	135.324	18.0093	126.358	5.51992	0.02 ± 0.01	1.15 ± 0.08
JZJ005	O=C1C=C(C2=CC=CN=C2)NC3=C(C4=CC=CC=C4)C(C(F) (F)F)=NN31	134.838	17.3623	124.461	12.7371	0.11 ± 0.01	1.19 ± 0.10
JZJ003	O=C1C=C(C2=CC=CC=N2)NC3=C(C4=CC=CC=C4)C(C(F) (F)F)=NN31	133.337	11.2184	122.789	15.9936	0.30 ± 0.06	1.09 ± 0.05
QO-31	O=C1C=C(C2=CC=CC=C2)NC3=C(C4=CC=CC=C4)C(C(F) (F)F)=NN31	133.241	7.5556	123.2	9.44925	0.18 ± 0.04	1.21 ± 0.09
V0546	COC1=CC=C(C2=NC(CN3CCN(C(C4=CC=C(C(C) (C)C)C=C4)=O)CC3)=NO2)C=C1	131.243	33.4441	139.418	21.7078	0.03 ± 0.01	1.11 ± 0.06
J2976	CC1=C(C(N2CCN(CC3=NOC(C4=CC=CC=C4)=N3)CC2)=O)C=CC(C)=C1	127.471	27.8648	131.678	23.1237	0.04 ± 0.02	1.06 ± 0.07
HW1	O=S(C1=CC=C(C2=C(C)ON=C2C3=CC=CC=C3)C=C1) (N ([H])C4=NC=NS4)=O	127.121	5.60496	121.763	−0.133443	0.02 ± 0.03	1.09 ± 0.07
S0412	CC1=CC=C(N2CCN(C(C3=NOC(C4=CC=C(F)C=C4)=N3)=O)CC2)C=C1	122.531	25.9099	126.206	24.5449	0.03 ± 0.07	1.03 ± 0.07
QO-66	O=C1C=C(CCl)NC2=C(C3=CC=C(Cl)C=C3)C(C(F) (F)F)=NN21	119.798	5.06265	101.894	3.78732	0.29 ± 0.02	–
QO-28	O=C1C=C(C(F) (F)F)NC2=C(C3=CC=CC=C3)C(C(F) (F)F)=NN21	116.979	6.81069	106.995	8.81548	0.09 ± 0.01	1.20 ± 0.09
QO-58	O=C1C=C(C2=C(Cl)N=C(Cl)C(F)=C2)NC3=C(C4=CC=CC=C4)C(C(F) (F)F)=NN31	115.719	7.43223	131.423	4.99359	0.47 ± 0.03	1.76 ± 0.09
QO-26	O=C1C=C(CCl)NC2=C(C3=CC=CC=C3)C(C(F) (F)F)=NN21	111.926	1.93944	103.058	4.26212	0.30 ± 0.04	1.03 ± 0.05
QO-72	O=C1C=C(C2=CC(F)=C(F)C(F)=C2F)NC3=C(C4=CC=CC=C4)C(C(F) (F)F)=NN31	106.616	6.21882	126.345	2.53901	0.48 ± 0.03	1.77 ± 0.08
QO-40	O=C [5]C=C(CCl)NC [1] = C(C [11](.) = CC=CC [19] = C@11C=CC=C@19)C(C(F) (F)F)=NN(@2)@6	104.384	−7.38669	107.642	−2.12664	0.07 ± 0.03	1.21 ± 0.10

−: no data. The bold data means the greatest effect in each channel.

proceed at ambient temperature for 2 h, then washed with an aqueous solution of sodium bicarbonate and brine. The organic phase was isolated, dehydrated using anhydrous sodium sulfate, and filtered. The resulting solution was evaporated to extract ethyl 4-(benzyl(ethyl)amino)-4-oxobutanoate (intermediate **1**, yield: 44.1%). Subsequently, 2-(3,4-dimethoxyphenyl)acetic acid (**SM3**) was dissolved in DCM; *N*,*N*-dimethylformamide (DMF) and oxalyl chloride were added and allowed to react at room temperature overnight. After completion of the reaction, the system was concentrated, dried, and set aside to obtain 2-(3,4-dimethoxyphenyl)-acetyl chloride (intermediate **2**). Subsequently, **SM4** and intermediate **1** were dissolved in acetonitrile, and the mixture was then added to a solution of sodium in ethanol while the temperature was controlled. The reaction was heated to 60 °C and incubated overnight. The acetonitrile was concentrated and removed, water was added, and the mixture was stirred and extracted. The organic phase was combined and dried with anhydrous sodium sulfate.

Tert-butyl4-(5-(3-(benzyl(ethyl)amino)-3-oxopropyl)-1,2,4-oxadiazol-3-yl)-methyl)piperazine-1-carboxylate (intermediate **3**) was obtained with an 81.5% yield. After dissolving intermediate **3** in DCM, trifluoroacetic acid (TFA) was added, and the mixture was stirred at room temperature until the reaction was complete, then concentrated to dryness. The resulting solution was purified by column chromatography to obtain *N*-benzyl-*N*-ethyl-3-(3-(piperazin-1-ylmethyl)-1,2,4-oxadiazol-5-yl)propanamide (intermediate **4**). Finally, the intermediate **4** was dissolved in DCM and stirred, followed by the addition of TEA. The temperature was then lowered to 0 °C, the DCM solution of the intermediate **2** was added, and the mixture was stirred overnight at room temperature. Water was added to the system after the completion of the reaction. The organic phase was washed twice, collected, and dried. It was then purified using column chromatography (DCM/MeOH) to acquire the final product, E0199 (4.32 g, yield: 51.3%. Fig. 2). The hydrogen and carbon spectra and mass spectra of E0199 are shown in Figs. S2–S4.

3.3. Effect of E0199 on Na_V channels

The typical traces of E0199 acted on $Na_V1.7$, $Na_V1.8$, $Na_V1.9$, $N_V1.5$, $Na_V1.4$, and $Na_V1.6$ channels in different concentrations (Fig. 3A). We observed the 10 μM CBZ channel inhibition ratio was 39.00% ± 8.01% for $Na_V1.7$ and 28.02% ± 14.11% for $Na_V1.8$, respectively (Fig. 3B). To observe the effect of E0199 on Na_V channels, we investigated whether 10 μM of E0199 could inhibit it. E0199 (10 μM) could inhibit Na_V currents with different ability, and the inhibition rates of $Na_V1.5$, $Na_V1.4$, $Na_V1.1$, $Na_V1.6$, $Na_V1.7$, $Na_V1.8$, and $Na_V1.9$ channels were 15.00% ± 6.90%, 1.07% ± 3.16%, 0.56% ± 1.14%, 1.17% ± 3.16%, 57.53% ± 4.50%, 75.33% ± 7.96%, and 46.82% ± 7.03%, respectively (Fig. 3C). The sequence of Na_V channel inhibition of E0199 at 10 μM was $Na_V1.8 > Na_V1.7 > Na_V1.9 > Na_V1.5 > Na_V1.6 > Na_V1.4 > Na_V1.1$ (Fig. 3C).

$Na_V1.7$, $Na_V1.8$, and $Na_V1.9$ are preferentially expressed in the sensory neurons of peripheral nerves and have been genetically validated in human pain syndromes [42–44]. We screened the above targets by conducting patch clamp activity at the cellular level and determined that the half maximal inhibitory concentration (IC_{50}) of E0199 inhibiting the $Na_V1.7$ channel was 0.52 ± 0.23 μM (Fig. 3D). Then, the activation and inactivation processes of E0199 on the Na_V channels were examined. Using 10 μM E0199, the activation curve of the $Na_V1.7$ channel was observed to shift from −33.65 ± 1.52 mV to −38.58 ± 2.11 mV, resulting in a 4.93 mV shift towards hyperpolarisation (Fig. 3E). E0199 (10 μM) caused a leftward shift in the inactivation curve of the $Na_V1.7$ channel, moving it from −69.55 ± 11.81 mV to −75.36 ± 8.81 mV. Additionally, it led to a hyperpolarisation shift of 5.81 mV along the same direction (Fig. 3F). We also observed the effect of E0199 on I–V curves of $Na_V1.7$ channel (Fig. 3G). E0199 (1 μM) could significantly inhibit the current density of $Na_V1.7$ channel at −10 mV, reducing the current density from −161.38 ± 7.39 pA/pF to −74.60 ± 7.71 pA/pF (Fig. 3H).

We found that the IC_{50} of $Na_V1.8$ channel was 0.24 ± 0.04 μM (Fig. 3I). The activation curve of the $Na_V1.8$ channel shifted from

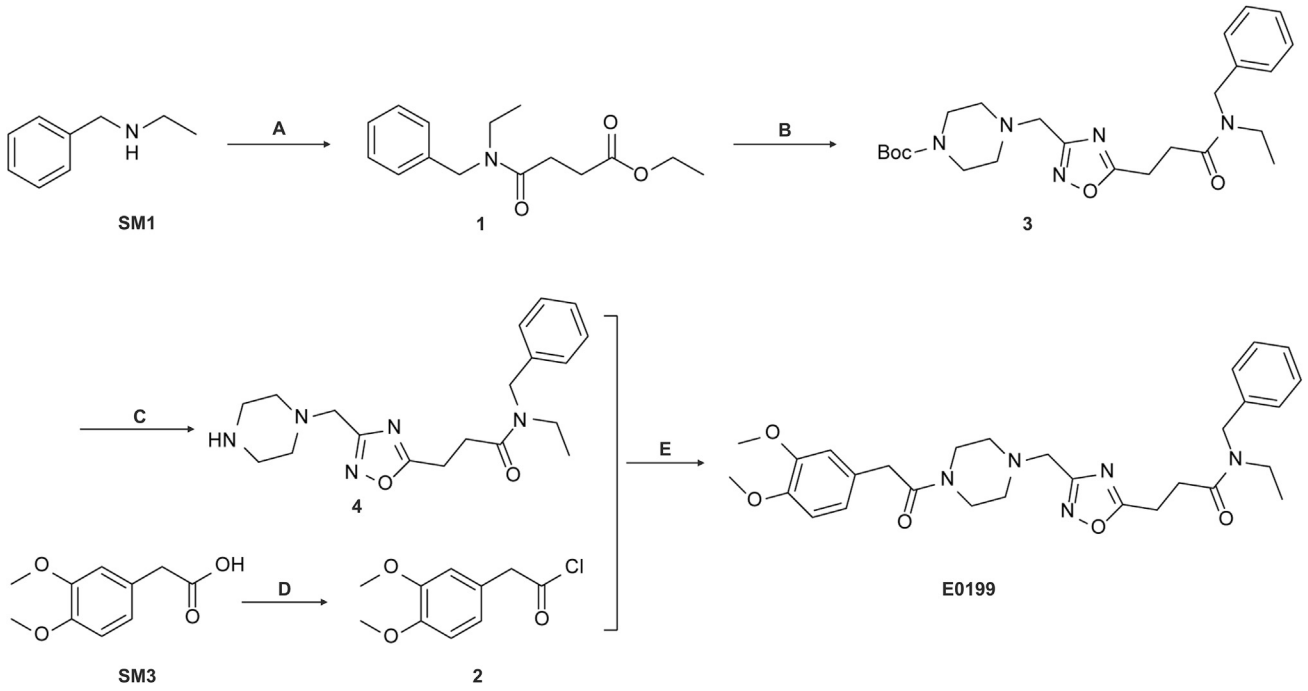

Fig. 2. Synthesis route of E0199: (A) Ethyl 4-chloro-4-oxobutanoate (**SM2**), dichloromethane (DCM), and triethylamine (TEA), 0 °C to room temperature, 2h; (B) *tert*-butyl (*Z*)-4-(2-amino-2-(hydroxyimino)ethyl)piperazine-1-carboxylate (**SM4**), CH_3CN, and EtONa, 60 °C, overnight; (C) DCM and trifluoroacetic acid (TFA); (D) oxalyl chloride and *N*,*N*-dimethylformamide (DMF), room temperature, overnight; and (E) DCM and TEA, 0 °C to room temperature, overnight.

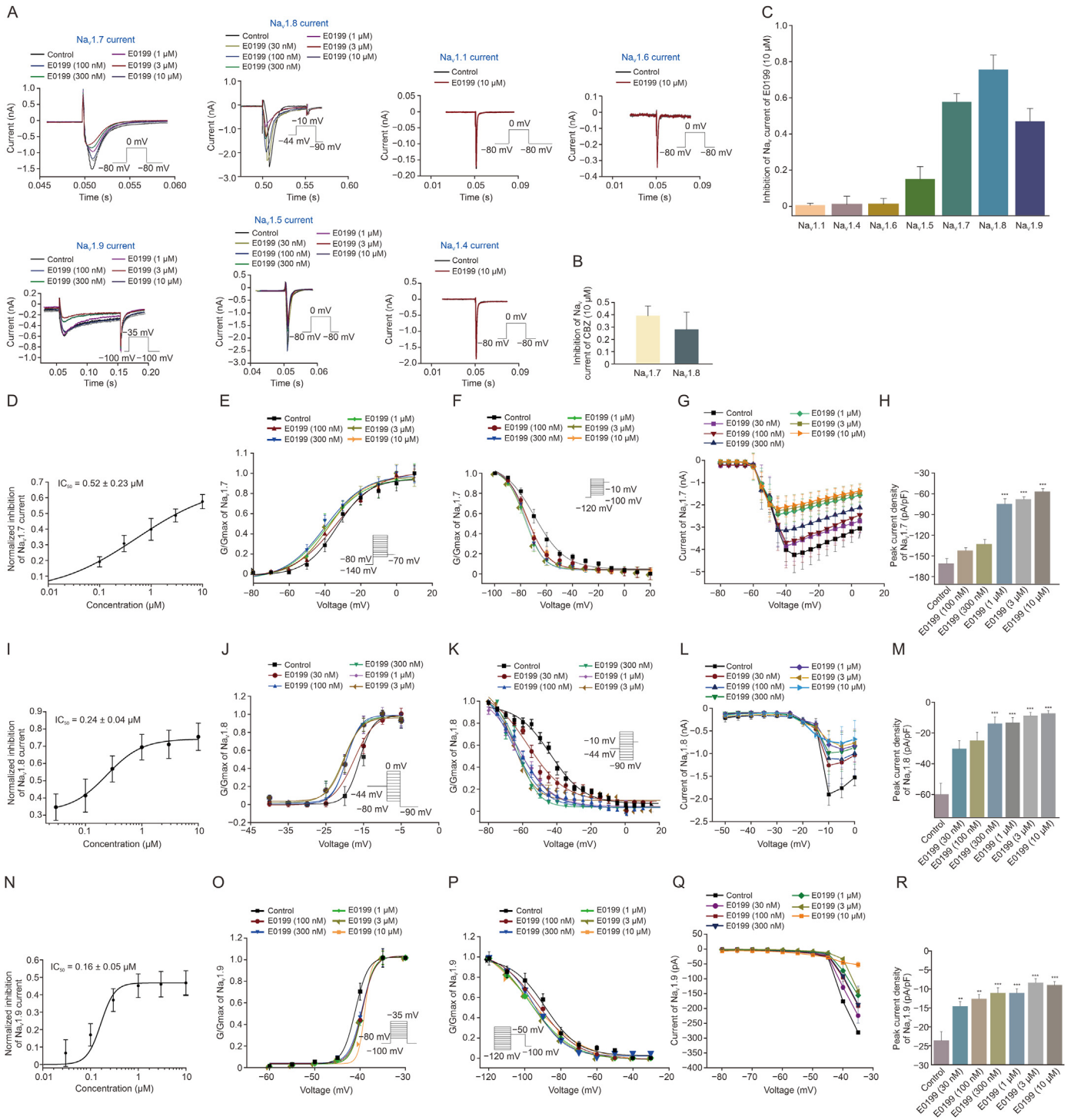

Fig. 3. Effect of E0199 on Na$_V$ channels. (A) Typical traces of the inhibition effect of E0199 on Na$_V$1.7, Na$_V$1.8, Na$_V$1.9, Na$_V$1.5, Na$_V$1.1, Na$_V$1.4, and Na$_V$1.6 channels at different concentrations. (B) Inhibitory effects of 10 μM of carbamazepine (CBZ) on Na$_V$1.7 and Na$_V$1.8 channels ($n = 6$ per group). (C) Inhibitory effects of 10 μM of E0199 on subtypes of Na$_V$ channels ($n = 8$ per group). (D) Concentration-dependent response curves of E0199 on Na$_V$1.7 channel currents ($n = 10$). (E) Influence of E0199 concentration on activation curves of Na$_V$1.7 channel ($n = 9$). (F) Influence of E0199 concentration on the inactivation curves of Na$_V$1.7 channels ($n = 9$). (G) Influence of E0199 concentration on the I–V curves of Na$_V$1.7 channels ($n = 9$). (H) Influence of E0199 concentration on peak current density of Na$_V$1.7 ($n = 6$). (I) Concentration-dependent response curves of E0199 on Na$_V$1.8 channel currents ($n = 9$). (J) Influence of E0199 concentration on activation curves of Na$_V$1.8 channel ($n = 6$). (K) Influence of E0199 concentration on the inactivation curves of Na$_V$1.8 channels ($n = 7$). (L) Influence of E0199 concentration on the I–V curves of Na$_V$1.8 channels ($n = 6$). (M) Influence of E0199 concentration on peak current density of Na$_V$1.8 channels ($n = 6$). (N) Concentration-dependent response curves of E0199 on Na$_V$1.9 channel currents ($n = 6$). (O) Influence of E0199 concentration on activation curves of Na$_V$1.9 channel ($n = 9$). (P) Influence of E0199 concentration on the inactivation curves of Na$_V$1.9 channels ($n = 8$). (Q) Influence of E0199 concentration on the I–V curves of Na$_V$1.9 channels ($n = 8$). (R) Influence of E0199 concentration on peak current density of Na$_V$1.9 channels ($n = 6$). Data are presented as mean ± standard error of the mean (SEM) and were analyzed by one-way analysis of variance (ANOVA)-Bonferroni test. Detailed information about the values and the statistical significance are presented in Table 2. $^{**}P < 0.01$ and $^{***}P < 0.001$, compared with control. Figs. 3D, I, and N using logisitic fitting and Figs. 3E, J, O, F, K, and P using Boltzmann fitting. IC$_{50}$: half maximal inhibitory concentration.

Table 2
The effects of E0199 on channels activation and inactivation of $Na_V1.7$, $Na_V1.8$, and $Na_V1.9$ channels.

Groups	$Na_V1.7$ $V_{1/2}$ (mV)				$Na_V1.8$ $V_{1/2}$ (mV)				$Na_V1.9$ $V_{1/2}$ (mV)			
	Activation	*n*	Inactivation	*n*	Activation	*n*	Inactivation	*n*	Activation	*n*	Inactivation	*n*
Control	−33.65 ± 1.52	10	−69.55 ± 11.81	10	−16.06 ± 1.19	13	−46.65 ± 1.46	15	−41.05 ± 1.41	14	−88.85 ± 8.69	13
E0199 100 nM	−35.78 ± 1.64	10	−74.98 ± 8.05	10	−17.52 ± 1.11	9	−54.39 ± 1.23**	11	−39.5 ± 1.35	9	−92.53 ± 11.79	9
E0199 300 nM	−40.01 ± 2.06	10	−76.02 ± 6.81**	10	−19.99 ± 1.84	9	−64.47 ± 10.06***	10	−39.61 ± 1.43	10	−94.55 ± 9.11	8
E0199 1 μM	−40.77 ± 2.01	9	−76.99 ± 7.18**	9	−20.35 ± 1.47	8	−62.42 ± 5.79***	11	−39.52 ± 1.26	9	−97.60 ± 12.80**	9
E0199 3 μM	−42.79 ± 1.71	9	−76.88 ± 6.91**	9	−20.16 ± 1.32	7	−67.19 ± 1.30***	12	−39.49 ± 1.24	10	−97.26 ± 11.61**	9
E0199 10 μM	−38.58 ± 2.11	9	−75.36 ± 8.81**	9	−19.59 ± 1.06	6	−62.80 ± 9.79**	8	−38.95 ± 0.73	11	−100.90 ± 19.07**	9

Data are presented as mean ± standard error of the mean (SEM) and were analyzed by one-way analysis of variance (ANOVA). $^{**}P < 0.01$ and $^{***}P < 0.001$, compared with control. $V_{1/2}$: voltage activation/inactivation midpoint.

16.06 ± 1.19 mV to the left to 19.59 ± 1.06 mV, resulting in a 3.53 mV shift towards hyperpolarisation (Fig. 3J). The inactivation curve of the $Na_V1.8$ channel shifted from −46.65 ± 1.46 mV to −62.80 ± 9.79 mV, resulting in a 16.15 mV shift towards the hyperpolarisation direction (Fig. 3K). We also observed the effect of E0199 on I–V curves of $Na_V1.8$ channel (Fig. 3L). E0199 (300 nM) observably inhibited the current density of $Na_V1.8$ channel at −10 mV. The current density decreased from −59.96 ± 7.19 pA/pF to −14.08 ± 4.21 pA/pF (Fig. 3M).

We also researched that the IC_{50} value for the blocking of the $Na_V1.9$ channel was 0.16 ± 0.05 μM (Fig. 3N). Additionally, the activation curve of the $Na_V1.9$ channel shifted from 41.05 ± 1.41 mV to the right to 38.95 ± 0.73 mV, resulting in a 2.1 mV shift towards polarisation (Fig. 3O). Similarly, the inactivation curve of the $Na_V1.9$ channel shifted from −88.85 ± 8.69 mV to −100.90 ± 19.07 mV towards the left and moved 12.05 mV in the direction of hyperpolarisation (Fig. 3P). We also observed the effect of E0199 on I–V curves of $Na_V1.9$ channel (Fig. 3Q). E0199 (30 nM) could signally restrain the current density of $Na_V1.9$ channel under −40 mV, and the current density decreased from −23.52 ± 1.66 pA/pF to −14.56 ± 1.19 pA/pF (Fig. 3R).

Thus, the sensitivity of E0199 to the Na_V channels was in the following order: $Na_V1.9$ > $Na_V1.8$ > $Na_V1.7$. The voltage activation midpoint ($V_{1/2}$) effects of other E0199 concentrations on the sodium channel activation curve are presented in Table 2. Based on the aforementioned results, E0199 had minimal impact on the Na_V channels activation curve shown above and did not significantly shift the activation curves of the $Na_V1.7$, $Na_V1.8$, and $Na_V1.9$ channels. E0199 induced the channel inactivation curves of $Na_V1.7$, $Na_V1.8$, and $Na_V1.9$ to shift towards the hyperpolarisation direction in a dose-dependent manner, as shown in Table 2. These findings indicated that E0199 primarily influenced the inactivation process of the $Na_V1.7$, $Na_V1.8$, and $Na_V1.9$ channels, facilitating channel inactivation and impacting the extent of the shift of the inactive curve in the sequence: $Na_V1.8$ > $Na_V1.9$ > $Na_V1.7$.

3.4. Effect of E0199 on K_V7 channels

The opening activities of E0199 on $K_V7.2$–$K_V7.5$ channels were observed at the cellular level. The degree of the opening of K_V7 channels appeared increasing in a dose-dependent manner. Typical traces of the effects of E0199 and RTG on K_V7 channels (Fig. 4A). The opening effects of RTG on K_V7 channels at 10 μM were as follows: 1.88 ± 0.06, 1.90 ± 0.08, 1.6 ± 0.07, and 1.37 ± 0.10 (Fig. 4B). The maximum opening degree of E0199 to the K_V7 channel was observed at 10 μM, and the opening multiple of E0199 for the $K_V7.2$ channel at 10 μM was 2.08 ± 0.1. The opening multiple of $K_V7.2/7.3$ channels was 1.23 ± 0.04, 1.30 ± 0.05 for $K_V7.4$ channels, and 1.80 ± 0.14 for $K_V7.5$ channels, but with minimal impact on $K_V7.1$ channels (Fig. 4C). Concentration for 50% of maximal effect (EC_{50}) of E0199 on $K_V7.2$ channels was 0.50 ± 0.07 μM (Fig. 4D). Effect of E0199 on I–V curves of $K_V7.2$ channel (Fig. 4E). E0199 at 10 μM concentration shifted the activation curve of $K_V7.2$ from −20.06 ± 1.42 mV to −50.44 ± 19.42 mV and a 30.38 mV shift in the direction of hyperpolarisation (Fig. 4F). E0199 (1 μM) could significantly increase the current density of $K_V7.2$ channel at −10 mV, from 8.49 ± 2.03 pA/pF to 21.56 ± 4.43 pA/pF (Fig. 4G).

Concentration for EC_{50} of E0199 on $K_V7.2/7.3$ channels was 12.78 ± 0.04 nM (Fig. 4H). Effect of E0199 on I–V curves of $K_V7.2/7.3$ channel (Fig. 4I). The activation curve of the $K_V7.2/7.3$ channel shifted left from −22.40 ± 3.52 mV to −53.45 ± 3.26 mV and moved 31.05 mV towards hyperpolarisation (Fig. 4J). E0199 (300 nM) could significantly increase the current density of $K_V7.2/7.3$ channel at −10 mV, from 21.71 ± 3.97 pA/pF to 50.15 ± 7.05 pA/pF (Fig. 4K).

Concentration for EC_{50} of E0199 on $K_V7.4$ channels was 0.19 ± 0.02 μM (Fig. 4L). Effect of E0199 on I–V curves of $K_V7.4$ channel (Fig. 4M). The activation curve of the $K_V7.4$ channel shifted from −15.32 ± 1.47 mV to −31.14 ± 1.54 mV and exhibited a 15.82 mV shift towards hyperpolarisation (Fig. 4N). E0199 (100 nM) observably increased the current density of $K_V7.4$ channel at −10 mV, from 35.05 ± 2.40 pA/pF to 59.78 ± 3.84 pA/pF (Fig. 4O).

Concentration for EC_{50} of E0199 on $K_V7.5$ channels was 27.14 ± 3.06 nM (Fig. 4P). Effect of E0199 on I–V curves of $K_V7.5$ channel (Fig. 4Q). The activation curve of the $K_V7.5$ channel shifted from −43.80 ± 1.09 mV to −68.16 ± 15.98 mV and moved 24.36 mV towards hyperpolarisation (Fig. 4R). E0199 (30 nM) significantly enhanced the current density of the $K_V7.5$ channel at −10 mV, from 11.77 ± 1.83 pA/pF to 19.82 ± 2.54 pA/pF (Fig. 4S).

Therefore, the sensitivity of E0199 to the K_V7 channel was in the order: $K_V7.2/7.3$ > $K_V7.5$ > $K_V7.4$ > $K_V7.2$. E0199 induced the activation curve of $K_V7.2$–$K_V7.5$, which shifted towards the hyperpolarisation direction in a dose-dependent manner, as shown in Figs. 4F, J, N, and R and Table 3. In summary, E0199 activates $K_V7.2$–$K_V7.5$ channels, moving their activation curve towards the hyperpolarisation direction and opening K_V7 channels. The order of mobility was $K_V7.2/7.3$ > $K_V7.2$ > $K_V7.5$ > $K_V7.4$.

3.5. Effect of E0199 on the excitability of DRG neurons in CCI model rats

The animals were divided into the following groups: control group, model group, 30 μM CBZ group, 10 μM RTG group, RTG (5 μM) + CBZ (15 μM) group, and various dose groups of E0199 (1, 3, and 10 μM). Step stimulation was used to observe the effect of each drug group on the number of AP. Compared with control group (under 500 pA stimulation), the number of APs in the model group increased from 3.11 ± 0.85 to 4.33 ± 0.12, and the amplitude increased from 94.25 ± 4.38 to 124.75 ± 1.76 mV. Rheobase decreased from 322.22 ± 64.80 to 188.24 ± 19.53 mV. The threshold decreased from −6.84 ± 2.51 to −15.94 ± 1.20 mV. The RMP was increased from −58.52 ± 1.47 to −49.42 ± 1.49 mV, indicating the successful modelling of the model group (Fig. 5).

Compared to the model group (under 500 pA stimulation), the AP numbers of the 30 μM CBZ, 10 μM RTG, RTG (5 μM) + CBZ

(15 μM), and 1, 3, and 10 μM E0199 dose groups decreased from 4.33 ± 0.12 to 2.67 ± 0.66, 2.33 ± 0.98, 1.67 ± 0.74, 0.49 ± 0.29, 0.30 ± 0.17, and 0.09 ± 0.05, respectively (Figs. 5A and B). E0199 at concentrations of 1, 3, and 10 μM E0199 showed more optimized inhibition of AP number than other groups. The AP amplitude of 30 μM CBZ, 10 μM RTG, RTG + CBZ, and 1, 3, and 10 μM of the E0199 dose group decreased from 124.75 ± 0.95 mV in the model group to 108.66 ± 2.03, 111.74 ± 0.36, 98.86 ± 1.66, 105.8 ± 1.14, 99.03 ± 1.30, and 96.6 ± 1.01 mV, respectively (Fig. 5C). E0199 (10 μM) inhibited the amplitude of AP better than the other groups.

The rheobase of the AP for the 30 μM CBZ, 10 μM RTG, RTG + CBZ, and 1, 3, and 10 μM E0199 dosing groups increased from 194.44 ± 18.91 pA in the model group to 333.33 ± 61.46, 375.00 ± 75.00, 400 ± 48.80, 375.00 ± 41.19, 400.00 ± 42.26, 442.85 ± 36.88 pA, respectively (Fig. 5D). E0199 at concentrations of 1, 3, and 10 μM was found to significantly increase the rheobase of CCI model mouse DRG neurons, whereas E0199 improved the rheobase better than the RTG + CBZ group (Fig. 5D). The peak width of AP was not significantly affected by the administration group (Fig. 5E). The AP threshold for the 30 μM CBZ, 10 μM RTG, RTG + CBZ, and the 1, 3, and 10 μM E0199 groups were increased from −15.85 ± 1.15 mV in the model group to −9.48 ± 2.72, −10.55 ± 1.88, −6.68 ± 1.19, −10.53 ± 2.34, −7.14 ± 2.34, and −4.30 ± 2.88 mV, respectively (Fig. 5F). The RTG + CBZ group, as well as the 3 and 10 μM E0199 groups, significantly increased the AP threshold (Fig. 5F). Notably, the threshold in the 10 μM E0199 group was higher than that in the RTG + CBZ group.

Furthermore, we measured the RMP, a parameter closely associated with K_V7 channels, and identified that the RMP of AP in the 30 μM CBZ, 10 μM RTG, RTG + CBZ, and the 1, 3, and 10 μM E0199 dose groups decreased from −49.42 ± 1.48 mV in the model group to −57.36 ± 4.28, −66.84 ± 3.58, −59.47 ± 0.74, −65.83 ± 2.68, −67.5 ± 2.69, and −67.96 ± 2.63 mV, respectively (Fig. 5G). The effect of the E0199 dose groups on AP RMP was better than that of the RTG group, and each dose of E0199 significantly increased RMP towards the hyperpolarisation direction. In summary, E0199 significantly influenced AP firing parameters in a dose-dependent manner, affecting the threshold, rheobase, amplitude, and RMP.

3.6. Impact of E0199 on pain behaviour in CCI model mice

The thresholds of thermal, cold, and mechanical withdrawal in the CCI models decreased significantly on Day 3 of modelling and stabilised by Day 9, and intervention therapy began on Day 11 (Fig. 6A).

The thermal withdrawal threshold of the 10 mg/kg RTG and RTG (5 mg/kg) + CBZ (10 mg/kg) groups was significantly increased on Day 11, and the effects of the 20 mg/kg CBZ and 1 5, and 20 mg/kg E0199 dose groups began to exhibit effects on Day 13. All treatment groups exhibited a consistent trend of increasing the thermal withdrawal threshold with subsequent administration. During treatment, 20 mg/kg E0199 increased the thermal withdrawal threshold to a greater extent than that in the RTG + CBZ and other groups (Fig. 6B and Table S2).

Subsequently, we observed the mechanical withdrawal threshold in the CCI model mice. The effect of 20 mg/kg E0199 became apparent on Day 11 and was superior to that of all other dosage groups. In both RTG + CBZ and 5 mg/kg E0199 groups, the effect occurred 13 days after drug administration, and the mechanical withdrawal threshold increased significantly. On Day 15, 1 mg/kg of E0199 showed a significant increase in the mechanical withdrawal threshold. Notably, the RTG (10 mg/kg) and CBZ (20 mg/kg) groups showed a slower onset of action with a significant increased in the mechanical withdrawal threshold on Day 17 (Fig. 6C and Table S3). Compared with the other treatment groups, 20 mg/kg of E0199 significantly alleviated mechanical hypersensitivity, exhibiting superior efficacy.

Then, we investigated the cold withdrawal threshold in CCI model mice. The RTG + CBZ group, along with the 1, 5, and 20 mg/kg of E0199 groups, demonstrated effectiveness starting on Day 11, exhibiting superior efficacy compared with the other groups. The RTG (10 mg/kg) and CBZ (20 mg/kg) groups exhibited efficacy starting on Day 13, resulting in a significant increase in the cold withdrawal threshold. Throughout the subsequent administration process, both the 20 and 5 mg/kg E0199 groups maintained higher cold withdrawal thresholds than other groups (Fig. 6D and Table S4).

Interestingly, for thermal withdrawal threshold within 15 days after treatment discontinuation, both the 5 mg/kg E0199 and RTG + CBZ groups maintained significantly higher thermal withdrawal thresholds than the model group (Fig. 6E). After discontinuation of treatment within 15 days, the 5 mg/kg E0199 group maintained a higher mechanical withdrawal threshold, whereas the RTG + CBZ group gradually approached the model group in terms of mechanical withdrawal threshold (Fig. 6F). After discontinuation of treatment within 15 days, the 5 mg/kg E0199 group and the RTG + CBZ group continued to maintain higher cold withdrawal thresholds than the model group (Fig. 6G). In conclusion, E0199 significantly alleviated thermal, mechanical, and cold hypersensitivity in CCI mice. The therapeutic effects persisted even after treatment discontinuation, and the efficacy of E0199 surpassed that of the combination drug group.

3.7. Impact of E0199 on locomotor behaviour in open field and elevated plus maze

Compared to the model group, both the E0199 and RTG + CBZ groups significantly prolonged the time and the distance of movement in the central open field. Each dose group of E0199 significantly enhanced the total distance and average speed of movement of CCI model mice in the open field (Figs. 7A–E). Additionally, we observed the effect of E0199 on the locomotor behaviour of the CCI model mice in an elevated plus maze. E0199 effectively improved the exploratory ability of CCI model mice in the elevated plus maze. E0199 at a dose of 20 mg/kg significantly increased movement time in the open arms and central zone compared to the model group, with no significant difference between the blank and sham surgery groups. The time spent in the open arms increased from 1.01 ± 0.41 s in the model group to 10.64 ± 1.40 s (Figs. 7F and G), and the movement time in the central area increased from 9.77 ± 2.34 s to 30.92 ± 7.42 s (Fig. 7H). There was no significant difference in total speed in zone in different groups (Fig. 7I). CCI model mice treated with E0199 at dosages of 1, 5, and 20 mg/kg showed a significant reduction in the proportion of movement time spent in the dark arms, reducing from 88.37% ± 3.06% to 67.51% ± 4.17% and 61.68% ± 2.99%, respectively (Fig. 7J). In conclusion, E0199 and RTG + CBZ treatments significantly enhanced movement in the central open field and improved exploratory behaviour in the elevated plus maze in CCI-induced mouse models.

3.8. Drug concentration of E0199 in the brain and DRG

The concentration in the brain was much lower than the concentration in DRG and plasma until 1 h after intravenous administration. E0199 demonstrated an average plasma drug concentration of 223.3300 ± 21.8000 ng/mL at 15 min, with drug content in the DRG measured at 0.1400 ± 0.0100 ng/mg and in

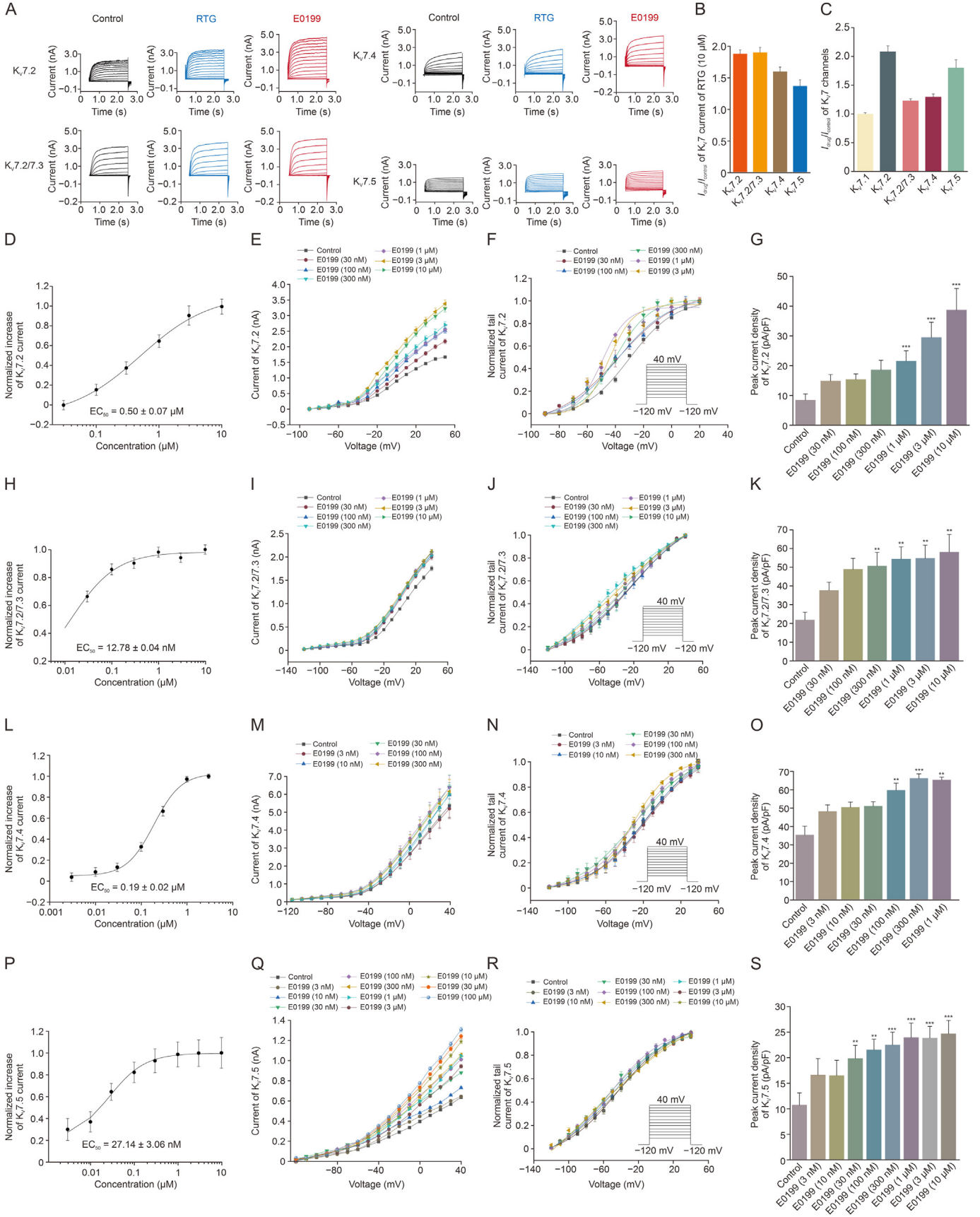

Fig. 4. Effect of E0199 on K_V7 channels. (A) Typical curves of influence of 10 μM of E0199 on $K_V7.2$, $K_V7.2/7.3$, $K_V7.4$, and $K_V7.5$ channels. (B) Current amplification of retigabine (RTG) (10 μM) for subtypes of K_V7 channels (n = 6 per group). (C) Current amplification of E0199 (10 μM) for subtypes of K_V7 channels (n = 6 per group). (D) Concentration-response

Table 3
The effects of E0199 on channels activation of $K_V7.2$–$K_V7.5$ channels.

K_V7 channels groups	$K_V7.2$ $V_{1/2}$ (mV)		$K_V7.2/7.3$ $V_{1/2}$ (mV)		$K_V7.4$ $V_{1/2}$ (mV)		$K_V7.5$ $V_{1/2}$ (mV)	
	Activation	*n*	Activation	*n*	Activation	*n*	Activation	*n*
Control	−20.06 ± 1.42	11	−22.40 ± 3.52	11	−15.32 ± 1.47	24	−43.80 ± 1.09	13
3 nM	–	–	–	–	−16.96 ± 1.16	10	–	–
10 nM	–	–	–	–	−19.01 ± 1.14	10	–	–
30 nM	–	–	–	–	−29.31 ± 1.64**	8	–	–
100 nM	−40.32 ± 22***	10	−21.12 ± 2.39	9	−28.34 ± 0.82**	8	−44.79 ± 3.01	9
300 nM	−39.87 ± 22**	10	−30.31 ± 2.81***	9	−31.79 ± 1.13***	6	−50.08 ± 1.52	6
1 μM	−39.97 ± 11.7**	9	−29.87 ± 1.82***	8	−31.93 ± 0.90***	6	−58.32 ± 1.72*	9
3 μM	−49.91 ± 14.63***	8	−41.91 ± 2.47***	8	−29.68 ± 1.44***	6	−54.26 ± 1.30*	6
10 μM	−50.44 ± 19.42***	7	−53.45 ± 3.26***	8	−31.14 ± 1.54***	6	−68.16 ± 15.98***	6

Data are presented as mean ± standard error of the mean (SEM) and were analyzed by one-way one-way analysis of variance (ANOVA). *$P < 0.05$, **$P < 0.01$, and ***$P < 0.001$, compared with control. –: no data. $V_{1/2:}$ voltage activation/inactivation midpoint.

brain tissue at 0.0046 ± 0.0004 ng/mg. Consequently, the plasma drug concentration was approximately 49264.7000 times higher than the brain concentration (Table 4), suggesting a low blood-brain barrier permeability of E0199 and indicating its predominant action in the periphery with minimal central nervous system side effects. Notably, the drug concentration in the DRG significantly exceeded that in brain tissue, and was being approximately 31.6200 times higher, implying that E0199's analgesic effects are primarily mediated through its action on the peripheral DRG. E0199 was <0.0900 detectable in liver tissue 1 h after administration, and was <0.0018 in kidney tissue after administration throughout the 2 h, indicating that E0199 does not accumulate in the liver and kidney, which means that E0199 may have low hepatorenal toxicity.

3.9. E0199 molecular dynamics simulation in $Na_V1.7$ and $K_V7.2$ channels

To better evaluate the binding of E0199 to the $Na_V1.7$ and $K_V7.2$ channels, we constructed the studied systems by molecular docking and performed 100 ns molecular dynamics simulations of the study system. Based on the equilibrium trajectories, we conducted the representative conformations comparison and energy profile analysis with CBZ and RTG as reference (Fig. 8A). All the studied systems could reach dynamic equilibrium after 50 ns, and both binding free energies and decomposition free energies were calculated based on the dynamic trajectories of 50–100 ns via molecular mechanics/generalized born surface area (MM/GBSA) approach. For the $K_V7.2$ system, the binding free energy of E0199 (−65.05 kcal/mol) was significantly superior to that of the positive control drug RTG (−38.03 kcal/mol). Similarly, for the $Na_V1.7$ system, the binding free energy of E0199 (−48.78 kcal/mol) was higher than that of the positive control drug CBZ (−25.57 kcal/mol) (Fig. 8B).

Based on the decomposition free energy analysis, the key amino acids (|energy contribution| ≥ 0.5 kcal/mol) that facilitate ligand binding were identified. Comparison of the binding of E0199 and RTG in $K_V7.2$ revealed that the residues located on chains A, C, and D contribute more to the energy of E0199 binding than RTG, especially the residues located on chain C (−12.92 vs. −4.94 kcal/mol) (Fig. 8C). Additionally, key amino acid W236 at the active site of the $K_V7.2$ receptor showed robust energy contributions in both the E0199 (−4.69 kcal/mol) and the RTG systems (−4.89 kcal/mol) (Fig. 8C). In addition, the binding of E0199 and CBZ on the $Na_V1.7$ receptor was compared. The total energy contribution of the key residues to E0199's binding to $Na_V1.7$ receptor considerably exceeded that of CBZ (−22.38 vs. −12.21 kcal/mol) (Fig. 8D).

In addition, E0199 formed strong π–π stacking interactions with F304 in chain A and F100, F104, and F112 in chain C of the $K_V7.2$ receptor. Additionally, E0199 engaged in strong hydrophobic interactions with L299 and I300 in chain A, L101 and V108 in chain C, and W236, F240, and L268 in chain D (Fig. 8E). In contrast, RTG formed strong π–π stacking interactions with F100 and F104 in chain C, and F240, and F305 in chain D of the $K_V7.2$ receptor, and also interacted hydrophobically with L299 and I300 in chain A by forming hydrogen bonds with W236 (Fig. 8F). Compared to RTG, E0199 could engage in additional hydrophobic interactions around the active pocket of the $K_V7.2$ receptor, suggesting greater stability in the binding site.

E0199 formed hydrogen bonds with Y1537 and R1602 and exhibited strong hydrophobic interactions with F1598, R1605, and I1588 of the $Na_V1.7$ receptor (Fig. 8G). As shown in Fig. 8H, CBZ could engage in π–π stacking interactions with F1598 and Y1573 in the $Na_V1.7$ receptor, along with hydrophobic interactions with V1541, M1582, and R1608. E0199 demonstrated stronger hydrogen bonding interactions with amino acid residues surrounding the active pocket than CBZ, suggesting more stable binding in the $Na_V1.7$ receptor relative to CBZ.

Our findings reveal that E0199, which exhibits superior binding free energy to both $K_V7.2$ and $Na_V1.7$ targets compared to RTG and CBZ, exhibits a relatively strong binding capacity to the receptors.

curves of E0199 on $K_V7.2$ channel currents ($n = 7$). (E) Effects of different concentrations of E0199 on the I–V curves of the $K_V7.2$ channels ($n = 7$). (F) Effects of E0199 concentrations on $K_V7.2$ activation curves ($n = 7$). (G) Influence of E0199 concentration on peak current density of $K_V7.2$ ($n = 6$). (H) Concentration-response curves of E0199 on $K_V7.2/7.3$ channel currents ($n = 8$). (I) Effects of different concentrations of E0199 on the I–V curves of the $K_V7.2/7.3$ channels ($n = 8$). (J) Effects of E0199 concentrations on $K_V7.2/7.3$ activation curves ($n = 8$). (K) Influence of E0199 concentration on peak current density of $K_V7.2/7.3$ ($n = 6$). (L) Concentration-response curves of E0199 on $K_V7.4$ channel currents ($n = 6$). (M) Effects of different concentrations of E0199 on the I–V curves of the $K_V7.4$ channels ($n = 6$). (N) Effects of E0199 concentrations on $K_V7.4$ activation curves ($n = 6$). (O) Influence of E0199 concentration on peak current density of $K_V7.4$ ($n = 6$). (P) Concentration-response curves of E0199 on $K_V7.5$ channel currents ($n = 6$). (Q) Effects of different concentrations of E0199 on the I–V curves of the $K_V7.5$ channels ($n = 6$). (R) Effects of E0199 concentrations on $K_V7.5$ activation curves ($n = 6$). (S) Influence of E0199 concentration on peak current density of $K_V7.5$ ($n = 6$). Data are presented as mean ± standard error of the mean (SEM) and were analyzed by one-way analysis of variance (ANOVA)-Bonferroni test. Detailed information about the values and the statistical significance are presented in Table 3. **$P < 0.01$ and ***$P < 0.001$, compared with control, Figs. 4D, H, L, and P using logisitic fitting and Figs. 4F, J, N, and R using Boltzmann fitting. EC_{50}: concentration for 50% of maximal effect.

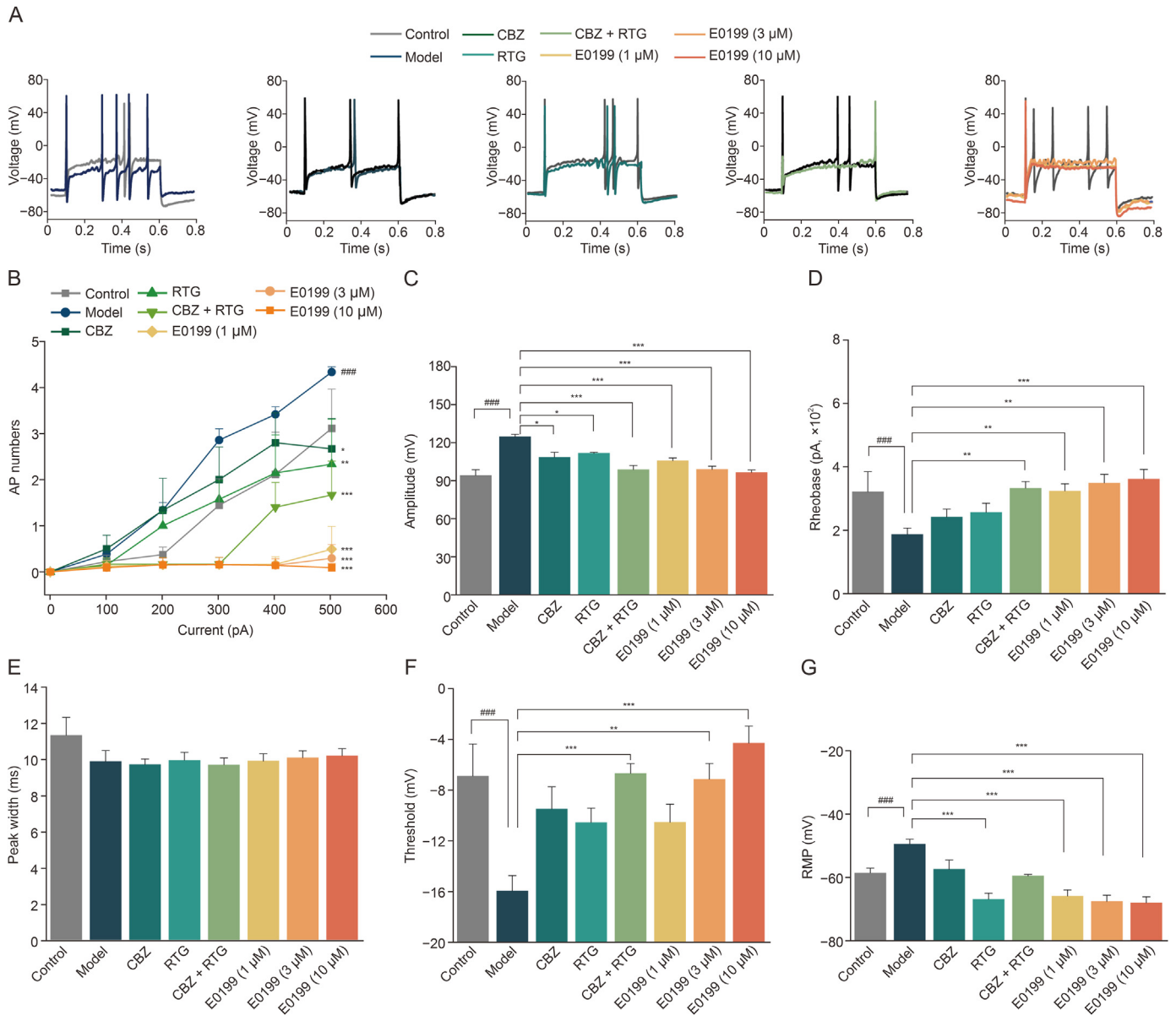

Fig. 5. Effects of E0199 on excitability parameters of L4–L6 dorsal root ganglia (DRG) neurons in chronic constriction injury (CCI) model rats. (A) Typical curves of the action potential (AP) of 30 μM carbamazepine (CBZ), 10 μM retigabine (RTG), RTG (5 μM) + CBZ (15 μM), and 1, 3, and 10 μM E0199 in the CCI model rat DRG neurons (500 pA). (B) Number of APs in the model and each treatment group under different intensities of current stimulation. (C) Amplitude of AP in the model group and each treatment group under 500 pA stimulation. (D) Rheobase for AP burst in the model group and each treatment group. (E) Peak width of AP in the model group and each treatment group under 500 pA stimulation. (F) AP thresholds of the model group and each treatment group under 500 pA stimulation. (G) Resting membrane potential (RMP) in the model group and each treatment group. Data are presented as mean ± standard error of the mean (SEM) and were analyzed by one-way analysis of variance (ANOVA)-Bonferroni test. $^{###}P < 0.001$, compared with control; $^{*}P < 0.05$, $^{**}P < 0.01$, and $^{***}P < 0.001$, compared with model group (ANOVA-Bonferroni test, $n = 8$ per group).

These findings, elucidated through molecular dynamics simulation, comprehensively explain the intrinsic mechanisms underlying the superior efficacy of E0199 compared to individual administration of the positive control drugs RTG and CBZ.

4. Discussion

The mechanism of NP is complicated, with abnormal electrical activity in the primary afferent nerve fibres that play a key role in NP following peripheral nerve injury. K_V7 and Na_V channels are widely distributed on neurons in the DRG, including small and medium-sized neurons innervated by unmyelinated C-fibres and thinly myelinated A-fibres, as well as large neurons innervated by Aβ-fibres. Channels such as $K_V7.2$, $K_V7.3$, and $K_V7.5$ are present in these neurons [27,45]. $Na_V1.7$, $Na_V1.8$, and $Na_V1.9$ are predominantly found in small- and medium-sized neurons innervated by nociceptive sensors, and $Na_V1.7$ is distributed in mechanosensitive large neurons [46]. Mutations leading to increased $Na_V1.7$ channel function are closely associated with erythromelalgia, paroxysmal extreme pain disorder, and small fibre neuropathy, whereas loss-

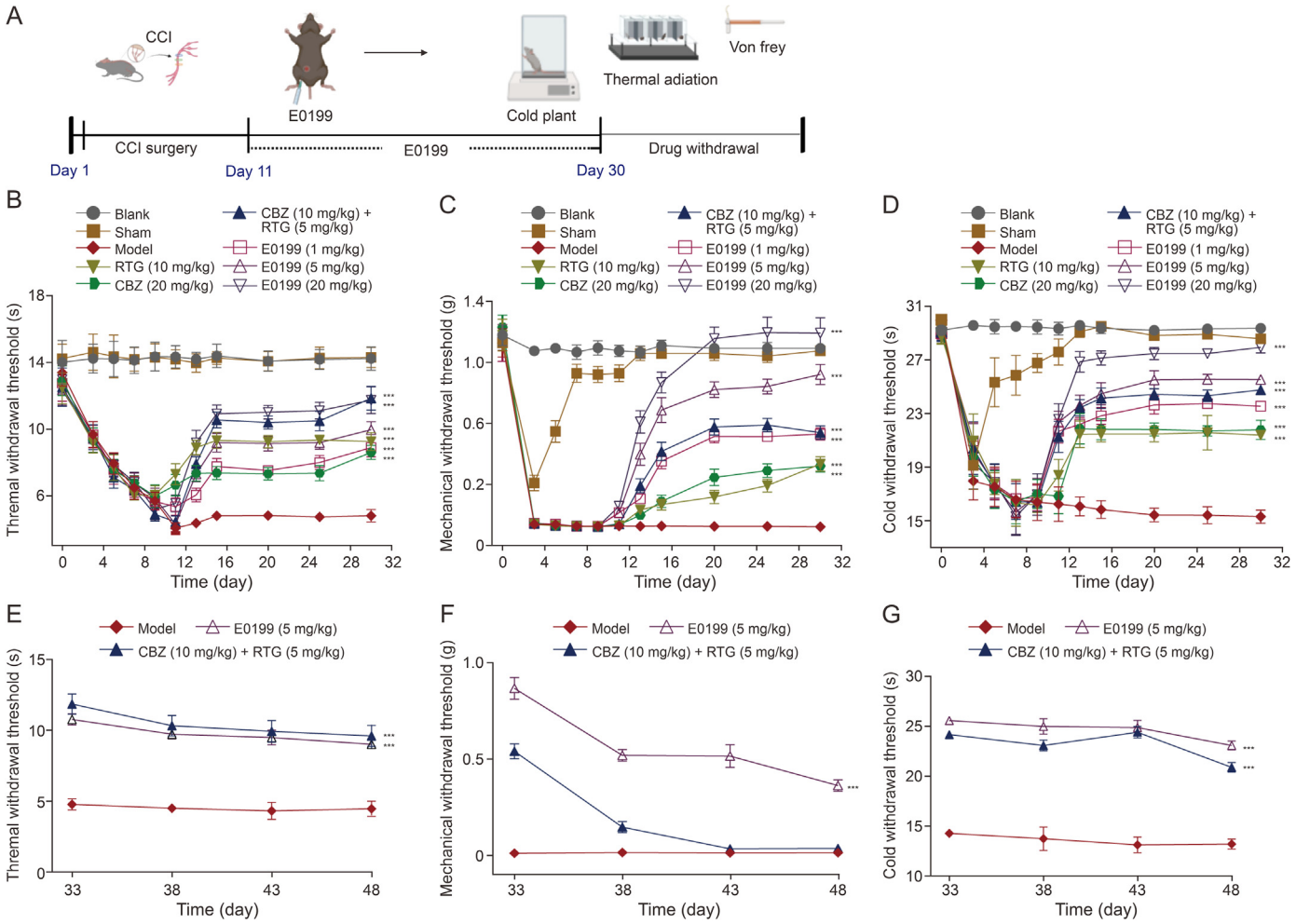

Fig. 6. Effect of E0199 on pain behaviour in chronic constriction injury (CCI) model mice. (A) Protocol of pain behaviour tests in CCI model mice. (B–D) Effects of 20 mg/kg carbamazepine (CBZ), 10 mg/kg retigabine (RTG), RTG (5 mg/kg) + CBZ (10 mg/kg), and E0199 (1, 5, and 20 mg/kg) on the thermal (B), mechanical (C), and cold (D) withdrawal thresholds in CCI model mice. (E–G) Changes in the thermal (E), mechanical (F), and cold (G) withdrawal thresholds 15 days after discontinuation of administration. Data are presented as mean ± standard error of the mean (SEM) and were analyzed by one-way analysis of variance (ANOVA)-Bonferroni test. $^{***}P < 0.001$, compared with model group ($n = 8$ per group).

of-function mutations are associated with painlessness, highlighting the crucial role of $Na_V1.7$ in pain modulation. NP resulting from nerve injury is closely linked to upregulation of Na_V channels and downregulation of K_V7 channels in the DRG. $K_V7.2/7.3$ and $Na_V1.7$ channels show co-localisation at the axon initial segment of myelinated fibres in peripheral DRG neurons [47], where the axon initial segment serves as the primary origin of NP signals [48]. Therefore, inhibiting Na_V channels and enhancing K_V7 channels may synergistically contribute to the treatment of NP.

Interestingly, ciguatoxins can induce cold allodynia in rodents by activating sodium channels and inhibiting potassium channels [49,50]. In animals with ciguatoxin-induced cold allodynia, lamotrigine and flupirtine effectively relieve pain [49], and alleviated cold allodynia caused by ciguatoxins [49]. In addition, lamotrigine and flupirtine can effectively open potassium ion channels while inhibiting sodium ion channel activity, demonstrating that the simultaneous modulation of sodium and potassium channels can effectively regulate NP. This case further illustrates that simultaneous modulation of sodium and potassium channels can effectively regulate the hypersensitivity induced by neurotoxins.

Advancements in resolution of the structures enable greater insights into the $Na_V1.7$ and $Na_V1.8$ channels [51,52], and the potential for the development of highly selective small-molecule compounds has become feasible [53]. However, clinical trial results for small-molecule blockers targeting $Na_V1.7$ and $Na_V1.8$ as single targets for pain treatment have yielded less than favourable outcomes [54]. Similarly, for K_V7 channels, the analysis of co-crystal structures with a batch of small-molecule compounds [55,56] revealed the activation mechanisms following the binding of small-molecule drugs to the channels [57,58]. Leveraging computer-aided drug design and artificial intelligence screening methods, we envision the development of a class of small-molecule compounds that simultaneously target K_V7 and Na_V channels, particularly focusing on their peripheral distribution. The design offers three key advantages: first, dual targeting synergistically boosts efficacy; second, focusing on peripheral targets minimizes the risk of central side effects; and third, aiming at the DRG as primary nociceptive sensory neurons eliminates the need for extensive blood-brain barrier penetration.

In our preliminary screening, we identified 210 candidate small-molecule compounds and verified their activities and relative

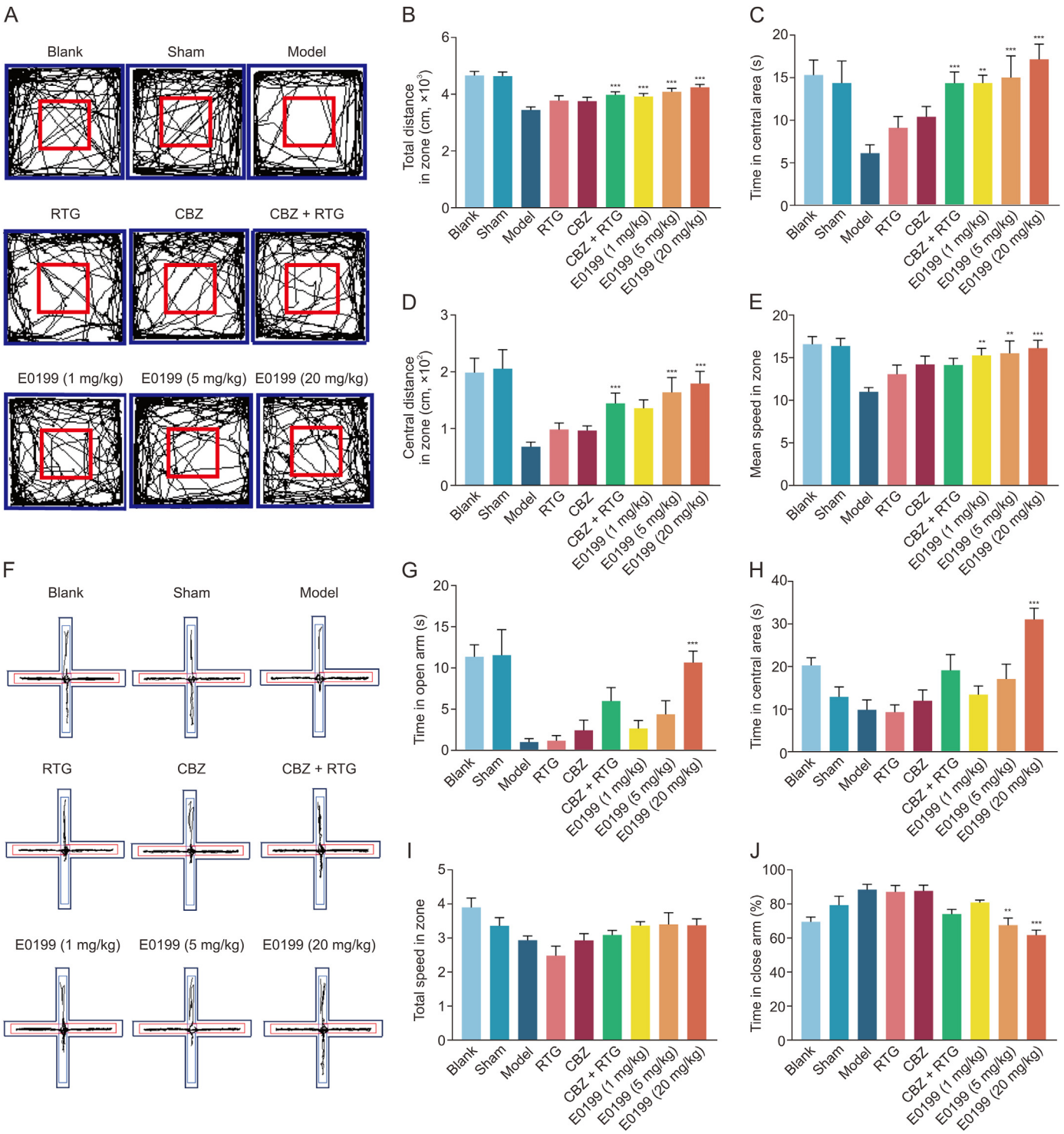

Fig. 7. Impact of E0199 on locomotor behaviour in open field and elevated plus maze. (A) Typical trajectories of each group of the chronic constriction injury (CCI) model mice in the open field. (B) Impact of E0199 on the total distance of the CCI model mice in an open field. (C) Effect of E0199 on the central movement time of the CCI model mice in an open field. (D) Impact of E0199 on the central distance of the CCI model mice in an open field. (E) Effect of E0199 on the mean motion speed of the CCI model mice in the open field. (F) Typical trajectories of each group of the CCI model mice in the elevated plus maze. (G) Effect of E0199 on open arm time in the CCI model mice. (H) Effect of E0199 on movement time in the central region of CCI model mice. (I) Effect of E0199 on the total speed of CCI model mice. (J) Effect of E0199 on close arm time in CCI model mice. Data are presented as mean ± standard error of the mean (SEM) and were analyzed by one-way analysis of variance (ANOVA)-Bonferroni test. $^{**}P < 0.01$ and $^{***}P < 0.001$, compared with model group ($n = 8$ per group). CBZ: carbamazepine; RTG: retigabine.

Table 4
The concentration of E0199 in rat plasma, dorsal root ganglia (DRG), brain, kidney, and liver at 5 min, 15 min, 0.5 h, 1.0 h, and 2.0 h.

Time Tissues	Concentration of E0199 (ng/mL in plasma, ng/mg in other tissues)				
	5 min ($n = 4$)	15 min ($n = 5$)	0.5 h ($n = 4$)	1.0 h ($n = 4$)	2.0 h ($n = 4$)
Plasma	1027.6700 ± 95.6900	223.3300 ± 21.8000	121.6700 ± 10.6800	6.0500 ± 1.0100	<0.2500
DRG	0.2800 ± 0.0320	0.1400 ± 0.0120	0.0920 ± 0.0017	0.0840 ± 0.0006	0.0770 ± 0.0030
Brain	0.0074 ± 0.0008	0.0046 ± 0.0004	0.0034 ± 0.0005	0.0024 ± 0.0001	0.0020 ± 0.0005
Kidney	<0.0018	<0.0018	<0.0018	<0.0018	<0.0018
Liver	0.0530 ± 0.0033	0.0240 ± 0.0037	0.0160 ± 0.0009	<0.0900	<0.0900

subtype selectivity for the most promising compound E0199 (Supplementary data, Figs. S1−S4, and Table S1). For the Na_V channels, E0199 exhibited a low IC_{50} for the $\Delta V_{1/2}$ of $Na_V1.8$ channels of inactivation, as low as, 33.1 ± 10.8 nM (Supplementary data and Fig. S5). For the K_V7 channels, E0199 demonstrated an EC_{50} order for channel opening as follows: $K_V7.2/3 > K_V7.5 > K_V7.4 > K_V7.2$, with remarkable sensitivity to $K_V7.2/3$ as low as 12.78 ± 0.01 nM. In terms of the degree of hyperpolarisation shift in the activation curves, E0199 demonstrated modulatory efficacy in the following order: $K_V7.2/7.3 > K_V7.5 > K_V7.2 > K_V7.4$. Additionally, E0199 exhibited a low EC_{50} for the $\Delta V_{1/2}$ of $K_V7.2/7.3$ channels, as low as 2.56 ± 0.46 μM (Supplementary data and Fig. S6). Above all, compound E0199 displayed obvious potential to $K_V7.2/7.3$, which contribute to M currents. Concurrently, the IC_{50} inhibitory activity of E0199 on the peripheral sodium channel is in the order of $Na_V1.9 > Na_V1.8 > Na_V1.7$. E0199 inhibited Na_V channels, which had a minimal impact on the activation curve but predominantly affected the inactivation curve, causing a shift in the inactivation curve in the following order: $Na_V1.8 > Na_V1.9 > Na_V1.7$. E0199 mainly affected peripheral sodium channels, such as $Na_V1.8$, $Na_V1.9$, and $Na_V1.7$, which play a more optimized role in regulatory activity and have a strong regulatory effect on TTX-resistant (TTX-R) sodium channels ($Na_V1.8$ and $Na_V1.9$). Summarily, E0199 exhibited excellent sensitivity in both K_V7 ($K_V7.2/7.3$, $K_V7.5$, and $K_V7.2$) and TTX-R Na_V channels ($Na_V1.8$ and $Na_V1.9$).

Although research labs worldwide are engaged in the development of analgesics targeting K_V7, $Na_V1.7$, $Na_V1.8$, and $Na_V1.9$, few small-molecule compounds have advanced to the clinical stage. RTG and flupritine were withdrawn from the market owing to severe adverse reactions, including blue-purple deposits in the retina and skin and liver damage [59,60]. Currently, no drugs targeting $Na_V1.7$ are available in the market. BIIB074 was discontinued after phase II clinical trials owing to its inferior efficacy compared to that of the placebo group [61]. PF-05089771 was also ineffective in treating diabetes-induced NP [15]. The development of analgesics targeting $Na_V1.7$ is exceedingly challenging. Despite considerable interest in the development of blockers targeting $Na_V1.8$, such as A-803467 and PF-01247324, the compounds targeting $Na_V1.8$ and $Na_V1.9$ channels have not yet been incorporated in clinical trials [62,63]. Based on this, our newly developed small-molecule compound targeted two types of channels, paving the way for the development of novel analgesics. Compared to most currently developed K_V7 channel openers, our compound (E0199) demonstrates excellent sensitivity with an EC_{50} activity superior to celecoxib, RTG, linopirdine, and other compounds, exhibiting EC_{50} as low as 0.50 μM [26,64]. Currently, there are no specific blockers for regulating the $Na_V1.9$ channel, and our compound, E0199, has a superior IC_{50} activity to block the $Na_V1.9$ channel compared to compounds such as bupivacaine, benzocaine, amitriptyline, and loperamide [65−67]. E0199 as a non-specific inhibitor for $Na_V1.8$ channel, still surpassed that of compounds vinpocetine, which was reported as an inhibitor of $Na_V1.8$ channel [68]. Therefore, E0199 simultaneously exerted potent regulatory effects simultaneously on K_V7 channels and $Na_V1.9$, $Na_V1.8$, and $Na_V1.7$ channels. E0199 changes the RMP of neurons by opening K_V7 channels and blocking peripheral $Na_V1.9$, $Na_V1.8$, and $Na_V1.7$ channels to stop APs. This is achieved by blocking $Na_V1.9$ channels in particular, which stop neurons from firing APs at low membrane potentials. This dual-channel modulation is a critical advantage of E0199 for inhibiting aberrant neuronal firing.

By opening the K_V7 channel, the new compound E0199 effectively lowered the RMP of neurons and prevented the abnormal discharge of DRG neurons in CCI model rats. In addition, it can modulate the rhythm of AP release by changing the rheobase and the threshold for AP burst. Notably, compound E0199 did not affect $K_V7.1$, human ether-a-go-go related gene (HERG) (Supplementary data and Fig. S7), or $Na_V1.5$ channels, which are widely distributed in the heart, nor did it affect the $Na_V1.4$ channel, which is prevalent in muscles, and does not affect the $Na_V1.1$ or $Na_V1.6$, which are distributed in the central nervous system (Fig. 3). By regulating the aforementioned ion channels, E0199 stabilises neuronal membranes, thereby effectively alleviating pain. E0199 exhibited significant therapeutic efficacy in mice with CCI-induced NP, with efficacy visible at a dose of 1 mg/kg (Supplementary data and Tables S2−S4). Besides, E0199 had a few effect on DRG excitability in normal animals, which indicated that E0199 was fairly safe (Supplementary data and Fig. S8). Moreover, E0199 significantly improved rodent performance in the rotarod and balance beam walking tests in the CCI model mouse (Supplementary data and Fig. S9). Additionally, E0199 did not affect social behaviours in mice or induce depression-like behaviours after administration (Supplementary data and Fig. S10). Furthermore, the acute toxicity of E0199 in CCI model mice was assessed, and median lethal dose (LD_{50}) was found to be 67.23 ± 0.50 mg/kg i.v., with the median toxic dose (TD_{50}) of 88.01 ± 1.41 mg/kg (i.p.) (Supplementary data and Fig. S11). After continuous administration, there were no abnormalities in 12 items of blood biochemistry in mice, suggesting that E0199 does not cause obvious liver and kidney damage in animals at the therapeutic dose, has few side effects, and is relatively safe (Supplementary data and Table S5). Based on molecular dynamics simulations, E0199 exhibited a stronger binding affinity for the receptors than RTG and CBZ. This result suggests that intrinsic factors may have contributed to the superior efficacy of E0199. Futhermore, E0199 had good cardiac safety at therapeutic doses (Supplementary data and Fig. S12). Most importantly, unlike other small-molecule compounds, E0199 demonstrates a low blood-brain barrier penetration rate and primarily acts on the peripheral system (Supplementary data, Tables 4, S6, and S7 and Fig. S13). This establishes a solid foundation for the regulation of peripheral NP. Therefore, E0199 exhibited an excellent safety profile and pharmacological activity both *in vitro* and *in vivo*.

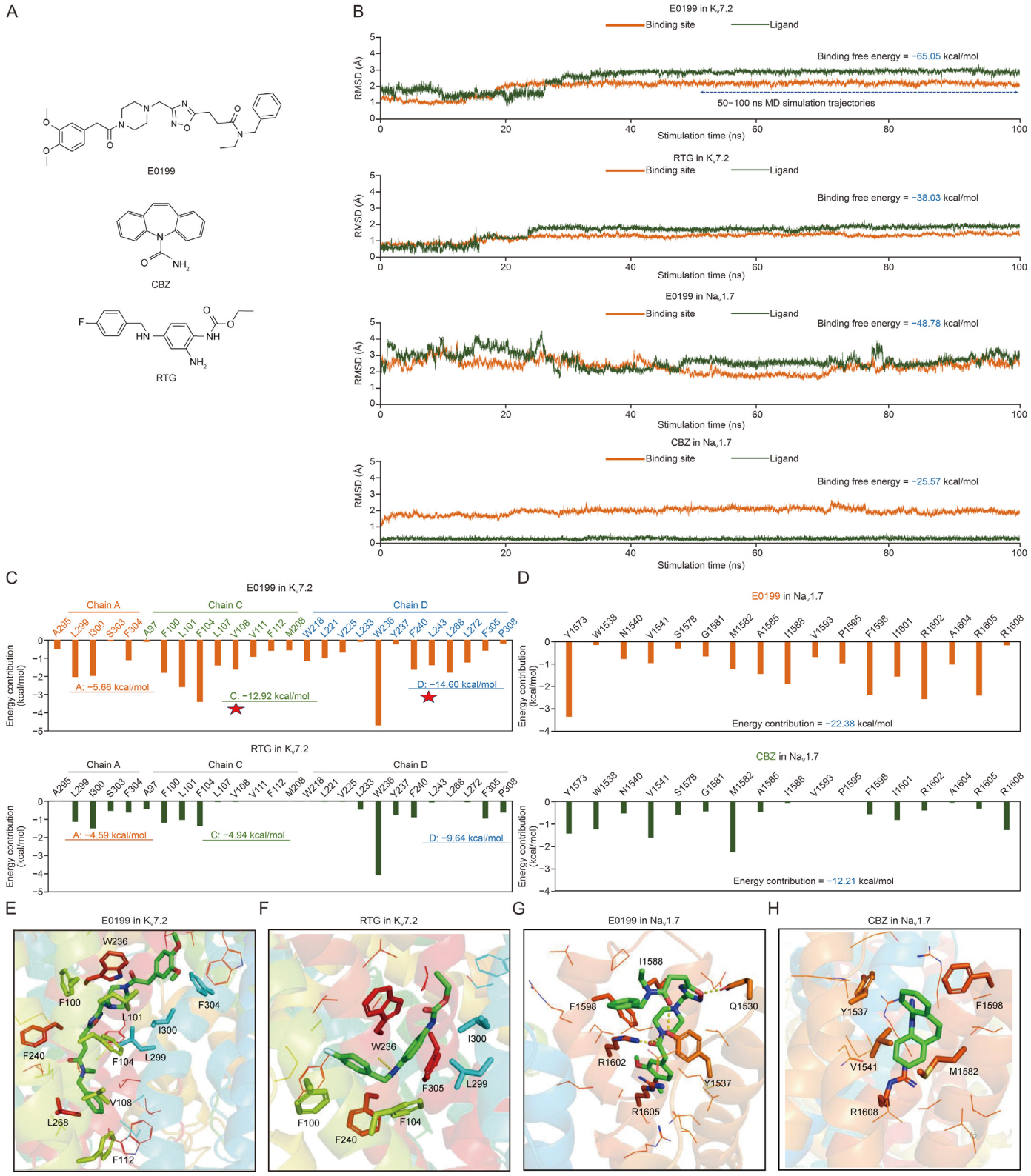

Fig. 8. Computational studies of E0199 in K_V7.2 and Na_V1.7. (A) Chemical structures of ligands in simulation systems. (B) Root-mean-square deviation (RMSD) analysis of the four simulation systems. (C) Analysis of decomposition free energy of E0199 and retigabine (RTG) in K_V7.2 systems. (D) Analysis of decomposition free energy of E0199 and carbamazepine (CBZ) in Na_V1.7 systems. (E, F) Representative conformations of E0199 (E) and RTG (F) in K_V7.2. (G, H) Representative conformations of E0199 (G) and CBZ (H) in Na_V1.7. The asterisk incicates that compared with RTG, E0199 is stable when combined with chains C and D. MD: molecular dynamics simulation.

5. Conclusion

We focused on developing novel small-molecule compounds that target both the Na_V channel inhibition and K_V7 channel activation, providing a new avenue for the development of small-molecule drugs for NP treatment. This approach offers a promising compound framework for the development of novel small-molecule analgesics and has significant scientific research value.

CRediT authorship contribution statement

Boxuan Zhang: Writing – review & editing, Writing – original draft, Visualization, Validation, Supervision, Resources, Project administration, Methodology, Investigation, Formal analysis, Data curation, Conceptualization. **Xiaoxing Shi:** Investigation. **Xingang Liu:** Investigation. **Yan Liu:** Investigation. **Xuedong Li:** Investigation. **Qi Wang:** Software. **Dongyang Huang:** Investigation. **Weidong Zhao:** Investigation. **Junru Cui:** Investigation. **Yawen Cao:** Investigation. **Xu Chai:** Investigation. **Jiahao Wang:** Investigation. **Yang Zhang:** Software. **Xiangyu Wang:** Writing – review & editing, Writing – original draft. **Qingzhong Jia:** Writing – review & editing, Writing – original draft, Conceptualization.

Declaration of competing interest

The authors declare that there are no conflicts of interest.

Acknowledgments

This study was funded by the Key Project from the Hebei Provincial Department of Science and Technology, China (Grant No.: 21372601D), the Foundation Postdoctoral Mobile Station of Basic Medical Sciences, Hebei Medical University, China (Grant No.: 20123120019), the Natural Science Foundation of Hebei Province, China (Grant No.: H2021206352), the Science and Technology Research Project of Colleges and Universities in Hebei Province, China (Grant No.: QN2023197), Hebei Medical University, Science and Technology, China (Grant No.: CYQD2023014), Hebei Provincial Department of Human Resources and Social Security, China (Grant No.: B2023003034), and the Consultative Foundation from Hebei Province, China (Grant No.: 2020TXZH01). We would like to thank Professor Zhaobing Gao from Chinese Academy of Sciences, China for providing us plasmid of $Na_V1.6$, as well as Professor Kewei Wang and Dr. Yani Liu from Qingdao University, China, who provided us stable cells expressing $Na_V1.4$ channel.

Appendix A. Supplementary data

Supplementary data to this article can be found online at https://doi.org/10.1016/j.jpha.2024.101132.

References

[1] N.B. Finnerup, R. Kuner, T.S. Jensen, Neuropathic pain: From mechanisms to treatment, Physiol. Rev. 101 (2021) 259–301.
[2] R. Baron, A. Binder, G. Wasner, Neuropathic pain: Diagnosis, pathophysiological mechanisms, and treatment, Lancet Neurol. 9 (2010) 807–819.
[3] R. Harbecke, J.I. Cohen, M.N. Oxman, Herpes zoster vaccines, J. Infect. Dis. 224 (2021) S429–S442.
[4] F. Guida, D. De Gregorio, E. Palazzo, et al., Behavioral, biochemical and electrophysiological changes in spared nerve injury model of neuropathic pain, Int. J. Mol. Sci. 21 (2020), 3396.
[5] S.P. Cohen, J. Mao, Neuropathic pain: Mechanisms and their clinical implications, BMJ 348 (2014), f7656.
[6] S.R.A. Alles, P.A. Smith, Peripheral voltage-gated cation channels in neuropathic pain and their potential as therapeutic targets, Front. Pain Res. (Lausanne) 2 (2021), 750583.
[7] J.E. Meents, E. Bressan, S. Sontag, et al., The role of $Na_V1.7$ in human nociceptors: Insights from human induced pluripotent stem cell-derived sensory neurons of erythromelalgia patients, Pain 160 (2019) 1327–1341.
[8] N.T. Blair, B.P. Bean, Roles of tetrodotoxin (TTX)-sensitive Na^+ current, TTX-resistant Na^+ current, and Ca^{2+} current in the action potentials of nociceptive sensory neurons, J. Neurosci. 22 (2002) 10277–10290.
[9] G. Goodwin, S.B. McMahon, The physiological function of different voltage-gated sodium channels in pain, Nat. Rev. Neurosci. 22 (2021) 263–274.
[10] C.G. Faber, G. Lauria, I.S. Merkies, et al., Gain-of-function $Na_V1.8$ mutations in painful neuropathy, Proc. Natl. Acad. Sci. U S A 109 (2012) 19444–19449.
[11] D.L.H. Bennett, C.G. Woods, Painful and painless channelopathies, Lancet Neurol. 13 (2014) 587–599.
[12] S.J. Middleton, I. Perini, A.C. Themistocleous, et al., $Na_V1.7$ is required for normal C-low threshold mechanoreceptor function in humans and mice, Brain 145 (2022) 3637–3653.
[13] E. Leipold, L. Liebmann, G.C. Korenke, et al., A *de novo* gain-of-function mutation in SCN11A causes loss of pain perception, Nat. Genet. 45 (2013) 1399–1404.
[14] J. Huang, C. Han, M. Estacion, et al., Gain-of-function mutations in sodium channel $Na_V1.9$ in painful neuropathy, Brain 137 (2014) 1627–1642.
[15] A. McDonnell, S. Collins, Z. Ali, et al., Efficacy of the $Na_V1.7$ blocker PF-05089771 in a randomised, placebo-controlled, double-blind clinical study in subjects with painful diabetic peripheral neuropathy, Pain 159 (2018) 1465–1476.
[16] S.M. Hoy, Lacosamide: A review of its use as adjunctive therapy in the management of partial-onset seizures, CNS Drugs 27 (2013) 1125–1142.
[17] B. Namer, D. Schmidt, E. Eberhardt, et al., Pain relief in a neuropathy patient by lacosamide: Proof of principle of clinical translation from patient-specific iPS cell-derived nociceptors, EBioMedicine 39 (2019) 401–408.
[18] P.J. Wiffen, S. Derry, R.A. Moore, et al., Antiepileptic drugs for neuropathic pain and fibromyalgia - an overview of Cochrane reviews, Cochrane Database Syst. Rev. 2013 (2013), CD010567.
[19] Y.-M. Zheng, W.-F. Wang, Y.-F. Li, et al., Enhancing inactivation rather than reducing activation of $Na_V1.7$ channels by a clinically effective analgesic CNV1014802, Acta Pharmacol. Sin. 39 (2018) 587–596.
[20] A. Mueller, H. Starobova, M. Morgan, et al., Antiallodynic effects of the selective $Na_V1.7$ inhibitor Pn3a in a mouse model of acute postsurgical pain: Evidence for analgesic synergy with opioids and baclofen, Pain 160 (2019) 1766–1780.
[21] S. Jo, H.B. Zhang, B.P. Bean, Use-dependent relief of inhibition of $Na_V1.8$ channels by A-887826, Mol. Pharmacol. 103 (2023) 221–229.
[22] H.J. Hijma, P.S. Siebenga, M.L. de Kam, et al., A phase 1, randomized, double-blind, placebo-controlled, crossover study to evaluate the pharmacodynamic effects of VX-150, a highly selective $Na_V1.8$ inhibitor, in healthy male adults, Pain Med. 22 (2021) 1814–1826.
[23] H. Okuda, S. Inoue, Y. Oyamada, et al., Reduced pain sensitivity of episodic pain syndrome model mice carrying a $Na_V1.9$ mutation by ANP-230, a novel sodium channel blocker, Heliyon 9 (2023), e15423.
[24] C.H. King, S.S. Scherer, $K_V7.5$ is the primary K_V7 subunit expressed in C-fibers, J. Comp. Neurol. 520 (2012) 1940–1950.
[25] J. Busserolles, C. Tsantoulas, A. Eschalier, et al., Potassium channels in neuropathic pain: Advances, challenges, and emerging ideas, Pain 157 (2016) S7–S14.
[26] X. Du, H. Gao, D. Jaffe, et al., M-type K^+ channels in peripheral nociceptive pathways, Br. J. Pharmacol. 175 (2018) 2158–2172.
[27] G.M. Passmore, A.A. Selyanko, M. Mistry, et al., KCNQ/M currents in sensory neurons: Significance for pain therapy, J. Neurosci. 23 (2003) 7227–7236.
[28] G. Blackburn-Munro, B.S. Jensen, The anticonvulsant retigabine attenuates nociceptive behaviours in rat models of persistent and neuropathic pain, Eur. J. Pharmacol. 460 (2003) 109–116.
[29] C.H. King, E. Lancaster, D. Salomon, et al., $K_V7.2$ regulates the function of peripheral sensory neurons, J. Comp. Neurol. 522 (2014) 3262–3280.
[30] F.M.C. Besag, M.J. Vasey, Neurocognitive effects of antiseizure medications in children and adolescents with epilepsy, Pediatr. Drugs 23 (2021) 253–286.
[31] F. Zhang, Y. Mi, J.L. Qi, et al., Modulation of K_V7 potassium channels by a novel opener pyrazolo[1,5-a]pyrimidin-7(4*H*)-one compound QO-58, Br. J. Pharmacol. 168 (2013) 1030–1042.
[32] Z.-Z. Xu, Y.H. Kim, S. Bang, et al., Inhibition of mechanical allodynia in neuropathic pain by TLR5-mediated A-fiber blockade, Nat Med. 21 (2015) 1326–1331.
[33] T.R. Cummins, S.D. Dib-Hajj, J.A. Black, et al., A novel persistent tetrodotoxin-resistant sodium current in SNS-null and wild-type small primary sensory neurons, J. Neurosci. 19 (1999), RC43.
[34] L. Tyrrell, M. Renganathan, S.D. Dib-Hajj, et al., Glycosylation alters steady-state inactivation of sodium channel $Na_V1.9$/NaN in dorsal root ganglion neurons and is developmentally regulated, J Neurosci 21 (2001) 9629–9637.
[35] I.F. Purchase, Ethical review of regulatory toxicology guidelines involving experiments on animals: The example of endocrine disrupters, Toxicol. Sci. 52 (1999) 141–147.
[36] J. Guillén, S. Robinson, T. Decelle, et al., Approaches to animal research project evaluation in Europe after implementation of Directive 2010/63/EU, Lab Anim. (NY) 44 (2015) 23–31.
[37] D.J. Wells, Animal welfare and the 3Rs in European biomedical research, Ann N Y Acad Sci. 1245 (2011) 14–16.

[38] Prepared by the Animal Facilities Standards Committee of the Animal Care Panel, Guide for laboratory animal facilities and care, ILAR J. 62 (2021) 345–358.
[39] F. Xu, L. Han, Y. Wang, et al., Prolonged anesthesia induces neuroinflammation and complement-mediated microglial synaptic elimination involved in neurocognitive dysfunction and anxiety-like behaviors, BMC Med. 21 (2023), 7.
[40] S. Zhang, Y. Jin, T. Liu, et al., SS-GNN: A simple-structured graph neural network for affinity prediction, ACS Omega 8 (2023) 22496–22507.
[41] M.J. Curtis, S. Alexander, G. Cirino, et al., Experimental design and analysis and their reporting II: Updated and simplified guidance for authors and peer reviewers, Br. J. Pharmacol. 175 (2018) 987–993.
[42] M. Alsaloum, S.G. Waxman, iPSCs and DRGs: Stepping stones to new pain therapies, Trends Mol. Med. 28 (2022) 110–122.
[43] D.L. Bennett, A.J. Clark, J. Huang, et al., The role of voltage-gated sodium channels in pain signaling, Physiol. Rev. 99 (2019) 1079–1151.
[44] S.D. Dib-Hajj, S.G. Waxman, Sodium channels in human pain disorders: Genetics and pharmacogenomics, Annu. Rev. Neurosci. 42 (2019) 87–106.
[45] M. Estacion, S. Liu, X. Cheng, et al., K_V7-specific activators hyperpolarize resting membrane potential and modulate human iPSC-derived sensory neuron excitability, Front Pharmacol 14 (2023), 1138556.
[46] S.D. Dib-Hajj, T.R. Cummins, J.A. Black, et al., Sodium channels in normal and pathological pain, Annu. Rev. Neurosci. 33 (2010) 325–347.
[47] A.I. Nascimento, T.F.Da. Silva, E.C. Fernandes, et al., Sensory neurons have an axon initial segment that initiates spontaneous activity in neuropathic pain, Brain 145 (2022) 1632–1640.
[48] A. Dorrego-Rivas, M.S. Grubb, The axon initial segment as a source of neuropathic pain, Brain 145 (2022) 1574–1575.
[49] K. Zimmermann, J.R. Deuis, M.C. Inserra, et al., Analgesic treatment of ciguatoxin-induced cold allodynia, Pain 154 (2013) 1999–2006.
[50] D.-Z. Wang, Y.-H. Xin, M.-H. Wang, *Gambierdiscus* and its associated toxins: A minireview, Toxins 14 (2022), 485.
[51] H. Shen, D. Liu, K. Wu, et al., Structures of human $Na_V1.7$ channel in complex with auxiliary subunits and animal toxins, Science 363 (2019) 1303–1308.
[52] X. Huang, X. Jin, G. Huang, et al., Structural basis for high-voltage activation and subtype-specific inhibition of human $Na_V1.8$, Proc. Natl. Acad. Sci U S A 119 (2022), e2208211119.
[53] Z. Li, Q. Wu, N. Yan, A structural atlas of druggable sites on Na_V channels, Channels (Austin) 18 (2024), 2287832.
[54] M. Alsaloum, G.P. Higerd, P.R. Effraim, et al., Status of peripheral sodium channel blockers for non-addictive pain treatment, Nat. Rev. Neurol. 16 (2020) 689–705.
[55] R.Y. Kim, M.C. Yau, J.D. Galpin, et al., Atomic basis for therapeutic activation of neuronal potassium channels, Nat. Commun. 6 (2015), 8116.
[56] X. Li, Q. Zhang, P. Guo, et al., Molecular basis for ligand activation of the human KCNQ2 channel, Cell Res. 31 (2021) 52–61.
[57] S. Liu, P. Guo, K. Wang, et al., General pharmacological activation mechanism of K^+ channels bypassing channel gates, J. Med. Chem. 65 (2022) 10285–10299.
[58] D. Ma, Y. Zheng, X. Li, et al., Ligand activation mechanisms of human KCNQ2 channel, Nat. Commun. 14 (2023), 6632.
[59] Y. Sun, Y. Gong, S. Lu, et al., Three-step synthesis of the antiepileptic drug candidate pynegabine, Molecules 28 (2023), 4888.
[60] A. Farcas, T. Balcescu, L. Anghel, et al., A description of medicines-related safety issues evaluated through a referral procedure at the EU level after 2012, Expert Opin. Drug Saf. 19 (2020) 755–762.
[61] J.M. Zakrzewska, J. Palmer, V. Morisset, et al., Safety and efficacy of a $Na_V1.7$ selective sodium channel blocker in patients with trigeminal neuralgia: A double-blind, placebo-controlled, randomised withdrawal phase 2a trial, Lancet Neurol. 16 (2017) 291–300.
[62] M.F. Jarvis, P. Honore, C.C. Shieh, et al., A-803467, a potent and selective $Na_V1.8$ sodium channel blocker, attenuates neuropathic and inflammatory pain in the rat, Proc. Natl. Acad. Sci. U S A 104 (2007) 8520–8525.
[63] C.E. Payne, A.R. Brown, J.W. Theile, et al., A novel selective and orally bioavailable $Na_V1.8$ channel blocker, PF-01247324, attenuates nociception and sensory neuron excitability, Br. J. Pharmacol. 172 (2015) 2654–2670.
[64] M. Borgini, P. Mondal, R. Liu, et al., Chemical modulation of K_V7 potassium channels, RSC Med. Chem. 12 (2021) 483–537.
[65] Z. Lin, S. Santos, K. Padilla, et al., Biophysical and pharmacological characterization of $Na_V1.9$ voltage dependent sodium channels stably expressed in HEK-293 cells, PLoS One 11 (2016), e0161450.
[66] J. Liang, X. Liu, J. Zheng, et al., Effect of amitriptyline on tetrodotoxin-resistant $Na_V1.9$ currents in nociceptive trigeminal neurons, Mol. Pain 9 (2013), 31.
[67] Y. Wu, B. Zou, L. Liang, et al., Loperamide inhibits sodium channels to alleviate inflammatory hyperalgesia, Neuropharmacology 117 (2017) 282–291.
[68] X. Zhou, X. Dong, J. Crona, et al., Vinpocetine is a potent blocker of rat $Na_V1.8$ tetrodotoxin-resistant sodium channels, J. Pharmacol. Exp. Ther. 306 (2003) 498–504.